A novel view on lubricant flow undergoing cavitation in sintered journal bearings

Bernhard Scheichl[1a,b,*], Ioana Adina Neacşu[1a], Alfred Kluwick[b]

[a] *AC²T research GmbH, Viktor-Kaplan-Straße 2D, A-2700 Wiener Neustadt, Lower Austria*
[b] *Institute of Fluid Mechanics and Heat Transfer, Vienna University of Technology, Tower BA/E322, Getreidemarkt 9, A-1060 Vienna, Austria*

Abstract

A new rational formulation of the cavitation phenomenon occurring in porous journal bearings in the regime of fully hydrodynamic lubrication is presented. The suitably extended form of the Reynolds equation is coupled with the semi-phenomenological Darcy's law so as to yield a proper description of the combined flow through the lubrication gap and the porous (sintered) seat, respectively. It is found that the initially unknown boundaries of cavitation give inevitably rise to gradual steepenings of the pressure gradients and the saturation of the lubricant at recondensation that finally form up to localised discontinuities. Hence, it is focussed on both theoretical foundations and an elaborate numerical investigation of the resultant lubrication problem. In order to determine the limits of applicability of this approach, specific investigations aim at evaluating the extreme cases of relatively low and high bearing loads, i.e. $\varepsilon \to 0$ and $\varepsilon \to 1\_$ where ε is the eccentricity ratio, and very long/short as well as highly porous/(almost) massive bearings. Here the effort is seen to be reduced by considering appropriate distinguished limits. The results include values of the friction coefficient obtained for various configurations and, most interestingly, point to a threshold value of ε above which the loss of numerical solutions indicates the loss of steady-state operation of the bearing. A first validation by in-house experiments proves satisfactory.

Keywords: Cavitation, Darcy flow, Hydrodynamic lubrication, Porous journal bearings

1. Introduction

When the friction forces between parts in relative motion have to be minimal, a thin layer of either oil, grease or solid particles is commonly introduced between the parts, as to avoid the undesired surface contact. In journal (i.e. slide) bearings this separation is accomplished by the action of hydrodynamic lubrication, where a fluid film that carries the load imposed on the bearing is formed as a result of the rotation of the eccentrically displaced journal. In conventional or massive bearings, this mechanism is maintained steadily through a localised supply of the lubricant, i.e. external reservoir of lubricant. In contrast, here we are interested in mass-preserving journal bearings, also referred to as self-lubricated bearings, which operate in a similar manner as classical journal bearings. The fundamental difference is the porous (sintered) seat: its impregnation with lubricant is necessary only once (at the beginning of the lifecycle of the bearing).

The literature on this subject is enormous and constantly growing, thereby expressing the thriving interest and demand for self-lubricated bearings by engineers. Manufacturing and application of porous journal bearings motivating much research in this direction, pondered in [1]. Unfortunately, an overview covering the most important developments in the reliable computational prediction of the behaviour of such systems and the underlying theoretical approaches is not existing, at least to the authors' knowledge. Therefore, in the following we just cite the publications considered most relevant and/or pioneering in terms of originality and classical but do not claim that this list is exhaustive in nature. The ultimate goal of this study is gaining a deepened understanding of the flow behaviour in self-lubricated bearings and hence a satisfactorily accurate prediction of their steady-state operation.

[1] see talk at the 39th Leeds–Lyon Symposium on Tribology (Great Challenges in Tribology), Leeds Trinity University College, 4–7 Sept. 2012

[*] Corresponding author, email: `scheichl@ac2t.at`, phone: +43-(0)2622-81600-158, fax: +43-(0)2622-81600-99

We therefore focus at a most simple self-consistent description of the physical mechanisms at play; shortcomings arising from non-rational modelling of the physics involved (though at a higher level of complexity) are avoided. To this end, some new/established theoretical aspects are in turn highlighted/revisited in greater breadth and depth as usually in the corresponding tribological literature. In this spirit, the present paper and fully numerical studies on the subject complement. Regarding the latter, the very recent one by Balasoiu et al. [2] serves as a useful example: they adopt the full governing equations for multiphase flow, supplemented with advanced semi-phenomenological closures. In contrast, the numerical analysis performed here and forming the central part of our study (Section 4)

- rests upon a careful, critical re-examination of the underlying physics on the different scales involved (Section 1),
- a thorough formulation of the lubrication problem involving the minimum number of non-dimensional groups (Section 2), which enables
- (as a side issue) a rigorous though preliminary analytical study dealing with several theoretical aspects of the problem not addressed previously (Section 3) and including
- (as an exciting novelty) the inevitable event of spontaneous recondensation, i.e. of saturation jumps, in steady-state operation of self-lubricated bearings (due to their periodic geometry),
- brings in a new efficient numerical strategy that copes with cavitation of an incompressible lubricant involving that phenomenon and tackles directly the steady-state operation (Section 4.1),
- eventually allows for a systematic parameter study and prediction of the bearing performance (Section 4.2),
- attended by an experimental validation (Section 4.3).

1.1. Self-lubrication of porous bearings

The basic principle behind the functioning of these type of bearings is that a porous network acts as a reservoir of the fluid so as to achieving a cohesive lubricant film In the loaded part of the bearing the lubricant is pushed into the porous channels of the seat, while the flow through the unloaded part contributes in refilling this lubrication gap [3]. Therefore, the main factor which influences the capability of storing and releasing lubricant is porosity, defined as the ratio between the void fraction and the total volume of the porous bearing. Common values for porosity lie between 20% and 35%, depending on the type of application (e.g. requiring a minimum of mechanical strength of the seat).

The porous network forming the seat consists of highly contorted and interconnected microscopic channels. The description of the creeping flow percolating through this entangled network on a macroscopic length scale, represented by the local distance $\tilde{r}$ from the centre of the seat, most commonly is based upon Darcy's law. It can be derived formally from the Stokes-flow assumption on the microscopic scale of a fluid (lubricant) with uniform dynamic viscosity $\tilde{\eta}$ and density by means of scale separation involving a proper homogenisation (averaging) process: we refer to the seminal papers [4–6] (and references therein). The thereby resulting quantities comprise the local porosity or void fraction ϕ of the sinter, the local flow velocity $\tilde{\boldsymbol{v}}$, and the difference $\tilde{p}$ between the local pressure and that in the (gaseous) environment of the bearing, $\tilde{p}_a$, taken as uniform:

$$\phi(\tilde{\boldsymbol{x}}) := \frac{1}{\tilde{V}_{\mathcal{S}}}\int_{\mathcal{S}} \Sigma(\tilde{\boldsymbol{x}}')\,\mathrm{d}\tilde{V}_{\mathcal{S}}\,,\quad [\tilde{\boldsymbol{v}},\tilde{p}](\tilde{\boldsymbol{x}}) := \frac{1}{\phi(\tilde{\boldsymbol{x}})\tilde{V}_{\mathcal{S}}}\int_{\mathcal{S}} [\tilde{\boldsymbol{v}}',\tilde{p}'](\tilde{\boldsymbol{x}}',\tilde{\boldsymbol{x}})\,\Sigma(\tilde{\boldsymbol{x}}')\,\mathrm{d}\tilde{V}_{\mathcal{S}}\,,\quad \tilde{\boldsymbol{x}}' = \frac{\tilde{\boldsymbol{x}}}{\sigma} \quad \text{for} \quad \sigma \ll \frac{\tilde{V}_{\mathcal{S}}(\sigma)^{1/3}}{\tilde{r}} \ll 1\,. \tag{1}$$

Herein primes indicate the quantities governing the microscopic flow process; the dependences on the macroscopic and microscopic space variables $\tilde{\boldsymbol{x}}$, $\tilde{\boldsymbol{x}}'$ having the reference lengths $\tilde{r}$ and the local one $\sigma\tilde{r}$ are stated explicitly. The first accounts for the variation of the flow due to the conditions holding at the surface of the porous network, the second introduces the ratio of the single length scale characteristic of the micro-structure of the network and $\tilde{r}$. Integration in (2) is carried out locally over the fraction of space $\mathcal{S}$ exhibiting a volume $V_{\mathcal{S}}$, defining an intermediate scale in the formal limit $\sigma \to 0$ associated with the homogenisation process. The characteristic or indicator function Σ in (1) assumes the values 1 or 0 depending on whether fluid is present at the position $\tilde{\boldsymbol{x}}$ or not. Hence, under the neglect of capillary effects as presumed subsequently, isolated cavities (lacking fluid) constitute the "foam" contribution to the porous network whereas the porosity ϕ as defined by (1) forms the complementary "sponge".

On the macroscopic scale, the inversion of the Stokes equation finally shows that in Darcy's law

$$\tilde{\eta}\,\phi\tilde{\boldsymbol{v}} = -\tilde{\boldsymbol{\Phi}}\cdot\nabla_{\tilde{x}}\tilde{p}\,, \tag{2}$$

now correctly including the porosity, the symmetric permeability tensor $\tilde{\boldsymbol{\Phi}}$ arises from the homogenisation process. Under the assumptions made above, this geometrical quantity is a functional of ϕ solely. However, due to the evidently practical (numerical) inaccessibility of the $\tilde{\boldsymbol{\Phi}}$-$\phi$-relationship it is the permeability rather than (2) one should term phenomenological. The scalar porosity is apparently much more susceptible to measurement than the permeability, i.e. the components of $\tilde{\boldsymbol{\Phi}}$, but this is of limited benefit in view of a reliable modelling of $\tilde{\boldsymbol{\Phi}}$. Nevertheless, a number of semi-empirical expressions and theories were proposed, among which the one advanced by Kozeny [7], here see also the classical textbook by Scheidegger [8], remains the most widely appreciated. His approach is based on the rough assumption that the porous medium is equivalent to a set of quite slender circular channels exhibiting varying area cross-sections embedded in a rigid matrix. The equation he derived expresses the dependence of the permeability on the specific overall surface area of the porous medium. However, many subsequent experimental studies, cf. [8], pp. 137–144, show severe deviations from the theoretical results. For this reason, formulating the individual components of $\tilde{\boldsymbol{\Phi}}$ and assigning the missing values to the arising parameters is still merely empirical at present; their reliable measurements are challenging. In many important cases, ϕ and, in turn, $\tilde{\boldsymbol{\Phi}}$ can be taken as homogeneous, i.e. constant (isopermeable material), and/or Darcy's law (2) as a locally orthotropic constitutive relationship. Then $\tilde{\boldsymbol{\Phi}}$ is represented only by its three diagonal components. In the commonly assumed case of a locally perfectly isotropic tensor $\tilde{\boldsymbol{\Phi}}$ it is even purely spherical and determined by the single scalar $\tilde{\Phi} = \mathrm{tr}(\tilde{\boldsymbol{\Phi}})/3$. In the most basic case of homogeneous isotropy this scalar is again a constant.

We emphasise that the extensions of (2) by Brinkman [9] (accounting for a smooth transition of the homogenised towards the cohesive flow adjacent to a porous surface) and in terms of the well-known Darcy–Brinkman–Forchheimer law (accounting for inertial effects) are definitely phenomenological if not inconsistent at all with the basic assumption of creeping flow. This motivates us to use Darcy's classical law in the form stated by (2). Applying the continuity equation $\nabla_{\tilde{x}} \cdot (\phi \tilde{\boldsymbol{v}}) = 0$ ensuing from the homogenisation process to (2) finally yields the equation

$$\nabla_{\tilde{x}} \cdot (\tilde{\boldsymbol{\Phi}} \cdot \nabla_{\tilde{x}} \tilde{p}) = 0 \tag{3}$$

governing the macroscopic or Darcy pressure. In case of isotropy, (3) reduces to Laplace's equation.

1.2. Cavitation in lubrication

The hydrodynamic pressure generated in the fluid film between a rotating shaft and a bearing was first considered rigorously by Osborne Reynolds in 1886. For what follows, the classical prerequisites of lubrication theory are adopted: a Newtonian lubricant in laminar flow where inertial forces are negligibly small compared to the viscous ones and a relatively thin lubrication gap. Consequently, from neglecting the inertia terms in the leading thin-layer approximation of the Navier–Stokes equations the Couette–Poiseuille velocity profile ensues; substituting this approximation for $\tilde{\boldsymbol{v}}$ in the continuity equation and integrating it across the gap height yields the familiar Reynolds equation, governing the Reynolds or lubrication pressure [10]. Most of the the subsequent lubrication models have been based on this equation, viewed as a milestone, ever since. However, this description is strictly valid only for an assumed fully coherent fluid film, as in the case of quite low values of the eccentricity ratio ($\lessapprox 0.5$). In reality, the lubricant often exhibits an almost discontinuous phase change from the initial liquid phase, when the hydrodynamic pressure drops significantly in the divergent part of the lubrication gap, even below the ambient pressure, usually and as here indicating atmospheric conditions, and for relatively moderate loads, i.e. eccentricities. This discontinuity associated with the sudden pressure decrease is referred to as cavitation. The possibility to incorporate the drop of the pressure below the ambient pressure has been the goal of much research, but due to the complexity of the underlying physics, this challenge has been mastered only insufficiently so far.

The critical quantity in lubrication is the local difference pressure $\tilde{p}$, all the more as the formation of local cavitation affects the overall behaviour of the bearing under varying conditions in a subtle manner. Here two main mechanisms have been identified in the literature, see the early study by Taylor [11] and the review by Dowson & Taylor [12]: cavitation is provoked either by

(i) the penetration of quite large amounts of gas (air) from the surroundings, thus favouring film rupture from the surface of the seat and accompanying the formation of a bubble or cavity so that $\tilde{p}$ varies only insignificantly about the zero-pressure level, or

(ii) an inner partial vaporisation of the lubricant in fully submerged (flooded) bearings into a mixture of liquid (containing dissolved gases as air) and vapour (and released gases), where $\tilde{p}$ may even take on correspondingly

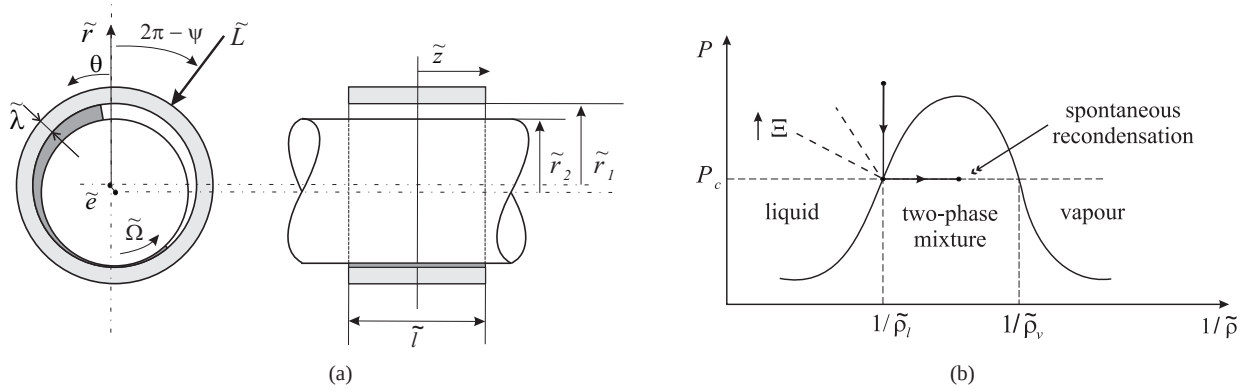

Figure 1: (a) geometrical configuration (shaded region indicates cohesive liquid lubricant), (b) phase diagram for the lubricant (compressibility parameter Ξ).

slight negative (subambient, i.e. subatmospheric) values. Under the assumption of isothermal and thermodynamically stable conditions and the neglect of dissolved gas, the cavitating lubricant can be advantageously considered as a homogeneous two-phase mixture exhibiting negligibly small pressure changes. We then arrive at the requirement $\tilde{p} \geq \tilde{p}_c$ with $\tilde{p}_c$ denoting the (in general) negative value of the pressure at vaporisation, i.e. cavitation.

In either case the same crucial question arises: *which is the correct (and unique) condition that describes the formation of cavitation both in a (from a rigorous* and *practical/computational point of view), sufficiently accurate* and *most simple manner?*

In order to reappraise the most popular preliminary answers to this question, we first specify the system to be investigated: here, the journal bearings are assumed to operate under stationary conditions with respect to the frame of reference attached to their (rigid) seat disposed in the bush. Their rigid rotating shaft is taken as impermeable, whereas the seat consists of a porous sintered matrix. The lubrication gap defined by the thin interstice separating these two parts is completely filled by the lubricant. Hereafter the position vector $\tilde{\boldsymbol{x}}$ is specified by the cylindrical coordinates $\tilde{r}$, θ, $\tilde{z}$ in the radial, circumferential or streamwise, and axial direction, respectively, and with the origin in the centre of the shaft: for a sketch of the configuration see Fig. 1(a). The subsequently interesting geometrical quantities comprise the inner radius of the (toroidal) seat $\tilde{r}_1$ and the radius $\tilde{r}_2$ of the shaft (having circular cross section). These form the gap clearance $\tilde{c} := \tilde{r}_1 - \tilde{r}_2$. Then the assumption

$$\tilde{c}/\tilde{r}_1 \sim \tilde{c}/\tilde{r}_2 \ll 1 \tag{4}$$

expresses the aforementioned slender-gap approximation. At this stage we also introduce the local (stationary) gap height $\tilde{h}$ and the streamwise velocity component $\tilde{u}$ of the lubrication flow.

All the existing cavitation models extending classical lubrication theory resort to the formulation of a boundary condition added to the Reynolds equation and governing the onset of cavitation at an initially unknown location. The latter is contracted to a curve in the $(\theta, \tilde{z})$-plane ($0 \leq \theta < 2\pi$), which renders the lubrication problem a free-boundary value problem. The simplest way to account for the occurrence of cavitation in lubricant flow is by keeping the gap pressure at the constant level required by one of the mechanisms (i) and (ii) in the regions where the solution of the Reynolds equation predicts lower ones otherwise. However, this so-called half-Sommerfeld or Gümbel boundary condition [10] lacks a sound theoretical justification and does not impose any restrictions on the original solution, subject to external boundary conditions (vanishing pressure $\tilde{p}$) further up- and downstream. As the Reynolds equation can be interpreted as the vanishing divergence in the $(\theta, \tilde{z})$-plane of the mass flux resulting from integration of a given velocity profile over the gap height, a more realistic condition has to provide continuity of that flux across that interface. The thereby resulting jump condition supplementing the Reynolds equation merely represents the weak formulation of the latter, and no new physics is introduced. Also, it then not only governs the onset but also termination of cavitation or, equivalently, the positions of the up- and downstream ends of the fully contiguous liquid film. For a

smooth distribution of the gap height $\tilde{h}$, the most general form of such a revised condition then reads

$$\frac{1}{\tilde{r}}\frac{\partial \tilde{p}}{\partial \theta} - \tilde{r}\frac{\partial \tilde{p}}{\partial \tilde{z}}\frac{\mathrm{d}\theta}{\mathrm{d}\tilde{z}} = \frac{6\tilde{U}\tilde{\eta}}{\tilde{h}^2}[1 - 2\varphi - (1-\varphi)S]\,, \quad S = \frac{\tilde{\rho}_m}{\tilde{\rho}_l}\,. \tag{5}$$

Here $\tilde{r}$ is identified with either $\tilde{r}_1$ or $\tilde{r}_2$ in view of the thin-gap assumption (4), $\tilde{\eta}$ is taken as the local dynamic viscosity of the liquid lubricant, $\tilde{U}$ denotes the (not necessarily stationary) shaft speed, and $\tilde{\rho}_l$, $\tilde{\rho}_m$ are the local densities of the liquid and the aforementioned mixture, respectively, with $S := \tilde{\rho}_m/\tilde{\rho}_l$ being the saturation of the latter ($0 < S \leq 1$). Furthermore, φ represents the fraction of the gap adjacent to the shaft that carries a liquid film of uniform velocity $\tilde{U}$ over the otherwise cavitating lubricant ($0 \leq \varphi < 1$). The gradient of $\tilde{p}$ is taken to be zero in the cavitation region. In the fully liquid phase, however, it approaches a negative/positive limit as expressed by the left-hand side of (5) in direction normal to the interface, having a local slope $\mathrm{d}\theta/\mathrm{d}\tilde{z}$ in the $(\theta, \tilde{z})$-plane, at the onset/termination of cavitation. In the region of cavitation or incomplete lubrication, S supersedes $\tilde{p}$ as the dependent variable governing the gap flow, whereas the value of φ has to be determined by an analysis taking into account capillary effects.

As early as in 1932, Swift [13] and Stieber [14] were the first who addressed the onset of cavitation in the spirit of (i). They neglected the continuation of a coherent liquid and, simultaneously, assumed a continuous initiation of gas entrainment as they set $\varphi = 0$ and $S = 1$. Then (5) reduces to the celebrated Reynolds boundary condition of Neumann-type governing the cavitation interface [10]. Later on, [11, 12], flow separation, triggered by an adverse pressure gradient acting in streamwise direction, was considered as the essential physical mechanism accompanying film rupture: its position and that of a vanishing shear rate $\partial\tilde{u}/\partial\tilde{r}$ at one of the solid facing surfaces forming the lubrication gap coincide. This criterion was investigated in the above studies for an infinitely long bearing entailing a planar flow with no $\tilde{z}$-dependence. When observed in the frame of reference fixed to one surface, here cavitation takes place in the divergent part of the lubrication gap slightly upstream of the location of its minimum height, and a liquid film moves under and/or above the cavity. The Couette–Poiseuille form of the flow then predicts film rupture where

$$\mathrm{d}\tilde{p}/\mathrm{d}\theta = 2\tilde{r}\tilde{\eta}\tilde{U}/\tilde{h}^2\,. \tag{6}$$

By combining this criterion, involving the local structure of the flow, with (5), arising from a contraction process, one could fix the position of cavitation in advance. However, consistency of this procedure has not been demonstrated so far. In contrast, Floberg [15] demonstrated how sub-cavity pressures imply film rupture further downstream. He was the first who considered this phenomenon as a rather abrupt transition from the coherent liquid film towards a ruptured one that moves as separated from the seat at rest by a cavity, filled entirely with air having negligible density with respect to the lubricant. This picture exactly leads to the condition (5), but with the restriction $S = 0$. In addition, Floberg also neglected the thickness of the ruptured liquid layer by setting $\varphi = 0$, so he assumed that cavitation affects the transverse section of the gap as a whole. This view is supported well by his own experiments and those conducted by Braun [16], who concluded it (out of all three proposed cavitation conditions outlined above) to reflect best the experimental findings. Additionally, his recent review [17] on the cavitation problem in bearings covers a vast amount of the cavitation models available in the literature, and represents a sound overview on the developments in this field.

It is stressed that the prediction of cavitation based on (5) disregards the frequently observed manifestation of cavitation in the form of spanwise fingering or individual streamers due to capillary effects ([15, 18], cf. [19]) and by inclusion of the resultant pressure jump in (5) (here Savage's work [20, 21] is among the forerunners, also of the associated stability analysis for both uniform and wavy spanwise cavitation fronts). For vaporous cavitation considered here, also the associated Gibbs–Thomson effect has not attracted attention in literature to the authors knowledge.

By critically evaluating the different ideas of modelling cavitation above, we abandon (6) as preference is given to the criterion (5), which has a clear physical meaning as it accounts for film rupture, see issue (i), and/or in combination with the inception of vaporisation, see issue (ii), and film reformation and/or recondensation self-consistently within the framework of lubrication theory. In the pure cases (i) and (ii) it has to be supplemented with the self-evident requirements $\tilde{p} = 0$ or $\tilde{p} = \tilde{p}_c$ (< 0), respectively. Interestingly, this criterion has apparently not attracted attention when the predominance of mechanism (ii) is presumed: here the inception of vaporisation requires the continuity of S, yielding $S = 1$, but spontaneous recondensation has to be regarded as the rule rather than the exception. Here the value of S jumps from one below 1 to 1 in downstream direction, accompanied by a jump in the pressure gradient from zero to that given by (5). For $\varphi = 0$ at both ends of cavitation (neglect of a remanent liquid layer), (5) is commonly referred to as Jakobsson–Floberg–Olsson (JFO) boundary condition: see [15, 22] and the references therein.

Most important, the pressure gradient vanishes at vaporisation but, in general, not at recovery. In summary, self-sustained lubrication subject to vaporisation cavitation in the circular gap is associated with two crucial properties:

(I) The Reynolds boundary condition definitely applies to film vaporisation but not to film reformation, i.e. recondensation;

(II) the distributions of pressure and saturation are smooth throughout except for an open curve in the $(\theta, \tilde{z})$-plane, associated with spontaneous recondensation as characterised by the gradual steepening of both the local increase of saturation up to the value 1 and the pressure gradient to non-zero values, which finally culminates in discontinuities.

2. Problem formulation

In this section we present the premises of the novel cavitation model that we employ in our study. We note that the flow in the journal bearing exhibits two forms of appearance, where the interaction between the two associated regions preserves the continuity of mass. In the current configuration, cavitation develops as a stable two-phase regime and expands in both axial and circumferential direction. Our main concern is with the determination of the gap pressure, including the formation of cavitation, under various load regimes.

2.1. Adopted cavitation model — requirements on lubricant

The lubricant is generally chosen according to various factors, including operation environment, lifetime, and the load-carrying capacity. However, the most influential criterion remains the frictional behaviour. Consequently, a large amount of research efforts is dedicated to developing novel lubricants with outstanding tribological properties. Preliminary tests have shown that ionic liquids exhibit an interesting low wear rate when used as lubricants. Additionally, their properties can be chemically altered and modelled as to their adaption to specific application necessities [23]. It is known that in journal bearings the vapour pressure of the lubricant plays an important role in the development of cavitation; hence the pure occurrence of mechanism (ii) addressed in Section 1.2 is favoured. In this respect, ionic liquids show interesting attributes: relatively low vapour pressures (which also means a correspondingly reduced tendency to evaporate over time). Apart from this, they exhibit good thermal stability and a satisfactorily weak dependence of the viscosity on temperature. These promising features motivates industry to choose them as prospective lubricants and us to adopt typical values of viscosity and vapour pressure of those liquids as input parameters for the numerical investigation. The sensitiveness of the operating range of the bearing to the variation of the vapour pressure is touched on quantitatively in Section 2.2.

It is reasonable to assume that the bearing is encapsulated in a solid casing, which implies that there is no lubricant leakage from the sinter to the exterior and air cannot enter the lubrication gap. Hence, we assume insulation of the toroidal cylinder comprising the seat and the gap at its facing sides and outer shell. In the absence of entrainment by external gases and under the assumption of an already degassed lubricant that undergoes a pressure drop down to its vapour pressure, the fluid will vaporise into a two-phase mixture composed of oil and vapour at varying concentrations. This event coins the notion cavitation in the spirit of (ii). Furthermore, it is reasonable to stipulate that the solid parts of the bearing take on the same temperature during operation and its relative increase in the lubricant film by viscous dissipation is negligibly small. The arrow attached to the solid curve in the phase diagram sketched in Fig. 1(b) indicates the resultant isothermal change of state of the lubricant passing the onset of vaporisation,

$$\tilde{p} = \tilde{p}(\tilde{\rho}) \tag{7}$$

with $\tilde{\rho}$ being the (variable) density of the lubricant. In the study at hand, we adopt the common assumption of an incompressible liquid phase, characterised by a uniform density $\tilde{\rho}_l$, and discard the possibility of complete vaporisation. Furthermore, let $\tilde{\rho}_v$, α_l, and x_l denote the densities of the lubricant at the state of saturated vapour as well as the, respectively, volumetric and mass fractions of the liquid phase. The quantity of pronounced variation in the region of cavitation is the saturation S, which then takes on values varying from $S_{min} = \tilde{\rho}_v/\tilde{\rho}_l$ to 1 and satisfies the well-known relationships

$$S = \alpha/x_l = \alpha_l + (\tilde{\rho}_v/\tilde{\rho}_l)(1-\alpha_l) = \left[x_l + (\tilde{\rho}_l/\tilde{\rho}_v)(1-x_l)\right]^{-1}. \tag{8}$$

Herein the second and the third expression for S reflect the mass-specific and volumetric compositions, respectively, of a fluid particle in the two-phase regime.

Cavitation by vaporisation is governed by the evolution of S in the two-phase region modelled as a homogenised mixture of both phases, according to (8). Albeit quite basic, this self-consistent extension of classical lubrication theory is seen to capture all the essential features of interest on a length scale comparable to the typical dimension (in $\tilde{r}$- and/or $\tilde{z}$-direction) of the lubrication gap.

2.2. Governing equations

Together with one of the radii $\tilde{r}_1$, $\tilde{r}_2$ and the gap clearance $\tilde{c}$ introduced in Section 1.2, the shaft eccentricity $\tilde{e}$, the bearing length $\tilde{l}$, and the radial thickness of the seat $\tilde{\lambda}$ define the geometry of the bearing. The resultant parameters are the eccentricity ratio $\varepsilon := \tilde{e}/\tilde{c}$ forming a key quantity as well as the aspect ratios $\Gamma := (2\tilde{r}_2/\tilde{l})^2$ and $\Lambda := \tilde{\lambda}/\tilde{r}_1$. The shaft rotates with a constant angular speed $\tilde{\Omega}\,(= \tilde{U}/\tilde{r}_2)$ about its axis in direction of the circumferential coordinate θ, and the bearing is considered to operate under stationary conditions. For these kinematic conditions we again refer to Fig. 1(a). Since we assume the configuration as isothermal and a not too large pressure increase, it is reasonable to take the viscosity $\tilde{\eta}$ as uniform. The behaviour of each the two flow regions identified in the system is captured by a separate equation governing the respective pressure, which are non-dimensional in the usual manner with the reference value

$$\tilde{p}_{ref} := 6\,\tilde{\Omega}\tilde{\eta}(\tilde{r}_2/\tilde{c})^2\,. \tag{9}$$

The first region is the thin gap between the shaft and bearing, filled entirely with the lubricant (submerged bearing). The displacement of the shaft from its original position due to rotation leads to the convergent/divergent gap of height $\tilde{h}$ or H when made non-dimensional with $\tilde{c}$. We neglect any tilt of the axes of the shaft and the seat and of noticeable roughness of its inner surface (due to its usual finishing and run-in) In the spirit of the central slender-gap approximation (4), H is then expressed by the well-known leading-order relationship

$$H(\theta) = 1 + \varepsilon\cos\theta\,, \tag{10}$$

which under the assumptions made even holds in case of high eccentricities, i.e. for $\varepsilon \to 1_-$. With $z = \tilde{z}/(\tilde{l}/2)$ and $P_R(\theta, z)$ and P_C being the distribution of the Reynolds pressure and the cavitation pressure, respectively, the Reynolds equation, suitably modified in order to cope with both cavitation and the ingestion of lubricant from the porous seat, is then written as

$$\frac{\partial}{\partial\theta}\left(H^3 S\,\frac{\partial P_R}{\partial\theta}\right) + \Gamma\,\frac{\partial}{\partial z}\left(H^3 S\,\frac{\partial P_R}{\partial z}\right) = \frac{\partial(HS)}{\partial\theta} - v_{D,r}\,. \tag{11}$$

It is supplemented with the three complementary conditions

$$P_R \geq P_C\,; \quad S = S(P)\,(\geq 1) \quad \text{as} \quad P_R > P_C\,; \quad S > 0\,. \tag{12}$$

Here the first is of Karush–Kuhn–Tucker-type and bounds the pressure by the cavitation pressure, and the second masters the application (11) to a compressible lubricant by the inversion of (7) in terms of an empirical, (on thermodynamic grounds) monotonically increasing function $S(P)$. Hence, one obtains the limit of perfectly incompressible flow of uniform density by characterising the fully liquid phase through the

$$\text{“incomopressible” specification of (12):} \quad P \geq P_C \quad \text{and} \quad S \equiv 1\,; \quad 0 < S < 1 \quad \text{and} \quad P_R \equiv P_C\,. \tag{13}$$

The flow behaviour in the two-phase regime is solely governed by the right-hand side of (11), which accounts for the variable saturation: $S_{min} \leq S(\theta, z) < 1$ in the region where $P \equiv P_C$. The representation of the flow in the lubrication gap by (11) subject to (12) or, specifically, (13) is more general than and, from the viewpoint of the numerical strategy pursued in the following, preferable to the original Elrod–Adams formulation [22, 24]. Elrod's original technique was then adapted successfully in the classical study by Meurisse & Giudicelli [25] to porous journal bearings, as well as taken up modified subsequently, e.g. in [26]: there a unit step function acting on the left-hand side of (11) and, for a strictly incompressible liquid phase, also on S in terms of a slack variable, provides the “switch” between

the single- and the two-phase regime. However, this modification still leaves P_R unspecified in the latter rather than it imposes its bounding from below by P_C as the conditions (12) do. In any case, that transition, here accounted for by (12) and even more (13), together with the initially unknown position of the liquid-/two-phase interface in the (θ, z)-plane ($0 \le \theta < 2\pi$, $0 \le z \le 1$), introduces a nonlinearity in the lubrication problem which proves delicate to deal with due to the sudden vanishing of the left-hand side of (11) in the sought limit of incompressible flow: see [27–29] (and the references therein). By handing over dominance of the elliptic operator to the advective one governing the wedge term on the right-hand side, having the characteristic lines $z = const$, this entails a rather weak coupling between the flow regions separated by the phase boundary.

The rightmost (source) term in (11) represents the radial inward mass flux or, complying with the assumption $S \equiv 1$ of uniform density of the lubricant inside the sinter, velocity component at the inner surface of the porous seat. The direction of mass exchange between the latter and the lubricant film by supply/leakage by percolation is given by its positive/negative sign. The appropriate boundary conditions for (11) are given by periodicity in θ, symmetry with respect to $z = 0$, and the prescription of the ambient pressure at the edge ($z = 1$) of the lubrication gap:

$$[P_R,\, \partial P_R/\partial\theta]_{\theta=0} = [P_R,\, \partial P_R/\partial\theta]_{\theta=2\pi}\,, \quad \partial P_R/\partial z\big|_{z=0} = 0\,, \quad P_R\big|_{z=1} = 0\,. \tag{14}$$

We note that a non-zero value of P_R at $z = 1$ due to the pressure jump caused by surface tension was addressed in [25], but a rational refinement of this boundary condition that accounts for a rigorous description of the toroidal liquid rings, sealing the gap and partly the seat by wetting as forming at their faces and driven by capillary and centrifugal forces, has not been carried out so far.

The second flow region is the bearing seat. Percolation through the porous matrix, i.e. the sintered seat, is governed by (3) when expressed in $r := \tilde{r}/\tilde{r}_1$, θ, z. Under the reasonable assumption of orthotropic permeability, this equation then takes on the form

$$\frac{1}{r}\frac{\partial}{\partial r}\left(r\,\Phi_r\,\frac{\partial P_D}{\partial r}\right) + \frac{1}{r^2}\frac{\partial}{\partial\theta}\left(\Phi_\theta\,\frac{\partial P_D}{\partial\theta}\right) + \Gamma\,\frac{\partial}{\partial z}\left(\Phi_z\,\frac{\partial P_D}{\partial z}\right) = 0\,. \tag{15}$$

Here $P_D(r,\theta,z)$ and the coefficients $\Phi_{r,\theta,z}(r,\theta,z)$ are, respectively, the distribution of the Darcy pressure referring to the lubricant in the sintered matrix and the non-vanishing diagonal components of $\boldsymbol{\Phi}$, denoted as $\tilde{\Phi}_{\tilde{r},\theta,\tilde{z}}$ when made non-dimensional with an appropriate reference value $\tilde{\Phi}_{ref}$. The latter are taken as input values and identified with unity in the frequently adopted case of homogeneous and isotropic permeability. The boundary conditions

$$\left[P_D,\, \frac{\partial P_D}{\partial\theta}\right]_{\theta=0} = \left[P_D,\, \frac{\partial P_D}{\partial\theta}\right]_{\theta=2\pi}, \quad \left.\frac{\partial P_D}{\partial z}\right|_{z=0} = \left.\frac{\partial P_D}{\partial z}\right|_{z=1} = \left.\frac{\partial P_D}{\partial r}\right|_{r=1+\Lambda} = 0\,. \tag{16}$$

associated with (15) account for periodicity, symmetry, and insulation of the seat.

It is noted that the pressure of the lubricant is continuous at the interface between the gap and the sinter. This is tied in with expressing $v_{D,r}$ by virtue of Darcy's law (2). Such a view is admissible only as long as the microscopic length scales given by the typical diameter of and distance between the pores in the surface of the seat are sufficiently small compared to the gap height. This enables a sufficiently smooth continuation of the macroscopic flow quantities, in the sinter given by (1), across the interface where the porosity then can be set to unity, cf. [30]. One should bear in mind that, even in the absence of surface roughness, a local gap height comparable with the micro-scales at play requires (11) to be replaced by a modification of the Reynolds equation that itself originates in an appropriate homogenisation process. However, under the assumptions adopted here Darcy's law finally establishes the still missing coupling conditions between the flow through the porous matrix and the lubrication gap by means of the requirements

$$r = 1\colon \quad P_R = P_D\,, \;\; v_{D,r} = K\,(\Phi_r\,\partial P_D/\partial r)(1,\theta,z)\,. \tag{17}$$

These requirements allow for interpreting (11) as a generalised Robin-type (mixed) boundary condition for (15) and spotting the conditions of periodicity either in (14) or in (16) as redundant. The parameter $K := 12\tilde{\Phi}_{ref}\tilde{r}_2/\tilde{c}^3$ proportional to the surface permeability is regarded as a quantity of $O(1)$ in terms of a distinguished limit and thus controls the strength of the coupling between the two flow regions. It is noteworthy that additive contributions $6(\tilde{c}/\tilde{r}_1)\Phi_\theta(1,\theta,z)H$ and $6(\tilde{c}/\tilde{r}_1)\Phi_z(1,\theta,z)H$ to the coefficients H^3 in the first and the second terms, respectively, on the left-hand side of (11) are neglected consistently in view of (4) and the reliable assumption that at the inner edge of the gap $|\Phi_\theta|$

Table 1: Non-dimensional parameters, their definitions and physical meanings.

Γ	Λ	P_C	ε	K
$(2\tilde{r}_2/\tilde{l})^2$	$\tilde{\lambda}/\tilde{r}_1$	$\tilde{p}_c/\tilde{p}_{ref}$	$\tilde{e}/\tilde{c}$	$12\,\tilde{\Phi}_{ref}\,\tilde{r}_2/\tilde{c}^3$
aspect ratio	thickness ratio	cavitation pressure	shaft offset, measures load	surface permeability

and $|\Phi_z|$ do not exceed $|\Phi_r|$ in their order of magnitude accordingly. These terms describe (microscopic) surface slips, satisfying the kinematic boundary condition, caused by the pressure gradients in the stream- and spanwise directions as implied by Darcy's law. This contrasts with several other approaches, see e.g. [25], where this effect of continuity of tangential speed at the gap/seat boundary is retained but proves numerically insignificant throughout as one expects (considering the adopted assumption of isotropic permeability). In addition, from here on $\tilde{\Phi}_{ref}$ is presumed to properly measure the magnitudes of all components of the permeability tensor throughout the sinter.

Neither the inception of vaporisation, nor the recondensation stages occur at previously known locations. In view of the subsequent analysis, it proves sufficient to close the resulting free-surface problem (10)–(17) by imposing the requirement of zero net mass flux across the gap/seat interface covered by the cavitation region (expressed by the area integral over $v_{D,r}$) and its boundary. This *global* condition provides a very weak coupling between the single-phase and the two-phase regions since it *not* necessarily implies *local* continuity of the mass flux normal to the interface, as given by (5). However, the validity of this local statement can be assumed tacitly as it arises automatically in terms of a weak formulation of the Reynolds equation (11), accomplished by its proper (conservative) numerical treatment. In account of the last paragraph of Section 1.2 as summarised by issues (I) and (II), reducing (5) to the here adopted JFO condition yields at

$$\text{incipient cavitation:}\quad P_R = P_C\,,\quad \frac{\partial P_R}{\partial\theta} = \frac{\partial P_R}{\partial z} = 0\,,\qquad \text{recondensation:}\quad P_R = P_C\,,\quad \frac{\partial P_R}{\partial\theta} - \Gamma\,\frac{\partial P_R}{\partial z}\,\frac{\mathrm{d}\theta}{\mathrm{d}z} = \frac{1-S}{H^2}\,. \tag{18}$$

This supplements (10)–(17) to a well-posed system of equations. For what follows, we seek solutions in the incompressible limit, specified by (13). The solutions consist of the distributions of the pressures $P_R(\theta, z)$, $P_D(r, \theta, z)$ as well as the saturation $S(\theta, z)$ on $0 \le z \le 1$ and $\theta \bmod 2\pi$. A rigorous proof for the existence and uniqueness of the solutions of a class of closely related problems concerning the distribution of P_R subject to an interface condition (18) is given by Boukrouche & Bayada [31], see also [27, 28]. However, the latter studies apply to massive bearings, i.e. the case $K = 0$, only and here to a limiting situation where the so-called Darcy problem given by (15) and (16) is solved once the so-called Reynolds problem defined accordingly by (10)–(14) has been solved. It is stressed that even then the problem considered here differs in details, mostly the missing ambient supply of lubricant at a prescribed part of the interface, sometimes forming a partially-flooded inlet, i.e. under "starved" conditions ($S < 1$). (Therefore, also a different numerical strategy is chosen.)

The solutions are parametrised by Γ, Λ, P_C, and the two key figures ε, K. As readily shown by inspection analysis followed by dimensional analysis, these five non-dimensional groups, highlighted in Table 1, represent an irreducible complete set of parameters entering the solution and uniquely determining the behaviour of the bearing. Notably, it is only the negative cavitation pressure P_C that is affected by viscosity as well as angular speed, according to (9).

The essential characteristic factors assessing the operation of the bearing are a Sommerfeld number *So*, here conveniently defined (according to Sommerfeld's original form rather than as its reciprocal, cf. [10], pp. 90–91) as the specific load, i.e. the ratio of the supplied bearing load $\tilde{L}$ that balances the force resulting from the lubrication pressure and the half of the projected active area, related to $\tilde{p}_{ref}$, the load attitude angle $\theta = \Psi$ of $\tilde{L}$ representing the displacement of the journal from its initial position, see Fig. 1(a), and the coefficient of friction μ or, when normalised with the small aspect ratio of the gap, μ_n, formed with the torque $\tilde{M}$ due to the shear stress exerted at the surface of the shaft by the Couette–Poiseuille flow:

$$[So,\,\mu,\mu_n] := \left[\tilde{L}/(\tilde{p}_{ref}\tilde{r}_2\tilde{l}),\;\tilde{M}/(\tilde{r}_2\tilde{L}),\;(\tilde{r}_2/\tilde{c})\mu\right] \quad \text{with} \quad [So,\,\Psi,\,\mu_n](\Gamma,\,\Lambda,\,P_C,\,\varepsilon,\,K) \tag{19}$$

calculated from the, in respect of the slender-gap approximation (4), leading-order relationships

$$[So\,\cos\Psi,\ So\,\sin\Psi] \sim \int_0^1 \int_0^{2\pi} [-P_R\cos\theta,\ -P_R\sin\theta]\,\mathrm{d}\theta\,\mathrm{d}z\,, \tag{20}$$

$$\mu_n \sim \frac{I_C + I_P}{So}\,, \quad I_C := \int_0^1 \int_0^{2\pi} S\,\frac{\mathrm{d}\theta\,\mathrm{d}z}{6H(\theta)}\,, \quad I_P := \int_0^1 \int_0^{2\pi} \frac{H(\theta)}{2}\,\frac{\partial P_R}{\partial\theta}\,\mathrm{d}\theta\,\mathrm{d}z\,. \tag{21}$$

In this sense, μ is an order of magnitude smaller than So, and the two contributions I_C and I_P originate in the Couette and the Poiseuille portion, respectively, of the flow. Moreover, in the region of cavitation the dynamic viscosity is given by the relationship $\alpha_l(S)\,\tilde{\eta}$, to be evaluated via (8). This drop of the viscosity is known to hold if the surface tension neglected here of the vapour bubbles is much smaller than the integral shear stresses in z-direction and fully consistent with a proper homogenisation process applied to the two-phase regime; we note that a more advanced modelling of the viscosity is proposed e.g. in [2]. Specifically, in (21) the volumetric filling degree of the liquid phase α_l is approximated by S with sufficient accuracy as $\tilde{\rho}_v\tilde{\rho}_l \ll 1$ can be assumed safely. We note that a slip effect due to the remanent liquid layer is neglected as $\varphi = 0$ in (5). Finally, it is obvious that So increases for increasing values of ε (cf. Table 1).

3. Some fundamental aspects of the lubrication problem

Before we turn to the numerical solution of the lubrication problem (10)–(17) in Section 4, six appealing attributes of it deserve attention. These are associated with several limits of the independent variables and the five independent system parameters (listed in Table 1) entering the solution, suitably coped with by perturbation analysis. Some of the results apply in the limit $K \to 0$, found as a regular one, only. Also, the onset of cavitation encountered in the following as affecting an infinitesimally small region motivates us to coin the notion of *marginal* cavitation. Here we assume that the solution of the problem is controlled by varying a certain member $\Pi(\Gamma, \Lambda, P_C, \varepsilon, K)$, say, of any set of five independent parameters formed with the original ones and keeping the remaining members fixed. Now let cavitation be initiated at a point in the (θ, z)-plane if Π exceeds a critical threshold Π^*, say. In this spirit, we speak of marginal cavitation when we consider the situation for rather small (positive) values of $\Pi - \Pi^*$.

We feel it is worth presenting the essential findings associated with those theoretical issues, although their analysis is not complete yet in all of the aspects and requires further effort. However, we anticipate that the numerical results put forward in Section 4.2 reproduce trends found from this preliminary theoretical analysis with convincing accuracy.

We are aware of the fact that this analysis supposedly appeals only the rather mathematically orientated reader. It complements the numerical study whereas the basic conclusions deduced from the latter can be understood without these technical details. Finally, given the length of the overall analysis presented, we positioned these in the Appendix A.

4. Numerical study

We now seek the numerical solution of (10)–(17), where our main focus lies on the parametrisation by the imposed load or, equivalently, on the eccentricity ε and the permeability parameter K. Furthermore, the so obtained Sommerfeld numbers, attitude angles, and coefficients of friction, see (20) and (21), are compared to those available from experiments and the thus established correlations evaluated.

4.1. Discretisation and iterative scheme

Conservation of mass at the interface between the liquid and the two-phase mixture is satisfied when a conservative finite-differences discretisation of (10)–(17) on an with S taken as the dependent variable is employed. We adopt second-order accuracy with the smallest control cell and stencils for central and forward/backward inside and at the boundary of the computational domain, respectively, possible (equivalent to a Keller–Box discretisation shifted about the half of its mesh size and a finite-volume representation). This ensures a proper resolution of the expected formation of a discontinuity in S. To ease the process of discretisation, we consider the mapping $(\theta, z) \mapsto (\theta_c, z_c)$ and work on a

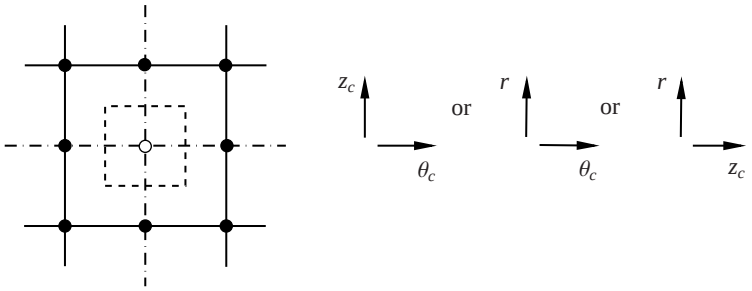

Figure 2: Grid stencil and control cell (dashed) in interior of computational domain: invariance with respect to any permutation/reflection of the coordinates, (11) and (15) to be satisfied at centre point (white circle).

mesh aligned with the coordinate directions with constant step size but variable number of grid points in the (θ_c, z_c)-space, hence referring to an accordingly unevenly spaced original grid: see Fig. 2. By this advanced scheme a smooth transition between the original fully conservative and an upwind (backward in θ-direction) second-order discretisation of the advective operator on the right-hand side of (11) at the cavitation boundary is facilitated. In anticipation of the detailed explanation of the method further below, the predominance of this operator over its elliptic counterpart in the cavitation zone is accomplished by an iterative adjustment of the P-S-relationship, which finally aims at splitting (11) into single equations of complementary type according to (12).

This modification advantageously avoids potential instabilities as e.g. the typical grid oscillations known from centrally formed discretisations of convection-diffusion equations in two coordinates. As found by a von-Neumann stability analysis, they occur for local grid Péclet numbers above a critical threshold. One could conceive an even more sophisticated procedure which establishes a dependence of the stencil on that number, but the approach we follow here proved sufficiently robust. Moreover, this strategy by far outweighs minor difficulties in case of an insufficient smooth switching between the two stencils at play. We also note that HS is a function of z solely for $K = 0$).

The bottleneck of all the known approaches targeted on the prediction of cavitation in an otherwise incompressible flow of a liquid lubricant results from the incorporation of a smooth pressure-saturation relationship $P_R = P_R(S\,;\Xi)$ according to (7), (12) in the numerical treatment: the parameter $\Xi > 0$ controls the herewith defined (positive) isothermal bulk compliance $S^{-1}\,\partial S/\partial P_R$, see the dashed lines in Fig. 1(b). Elrod & Adams [24], see also [22], were the first who introduced such a relationship statically in their conservative numerical marching scheme coping first with cavitation in bearings, with a discretisation alike the second-/first-order approach outlined above; yet, the method they proposed proves unacceptable from a more strict numerical point of view due to an apparent loss of stability when the limit of an incompressible liquid phase — the prediction of which is desired as a matter of course — is approached, according to (13). These authors obtained converged steady-state solutions by considering an extended unsteady problem and adopting an alternating-direction implicit (ADI) scheme, where advancing in time in each half time step is accomplished by an implicit Euler scheme. However, this is unconditionally stable insofar as the associated ordinary differential equation is stable and as long as a finite compressibility is taken into account. One should also note that their method was originally applied to tapered slider bearings [22], see also Sahlin et al. [32]. In [22] the positions of discontinuities associated with recondensation are fixed by those of the grooves bounding the regions of an lubrication-induced pressure increase but do not occur spontaneously as in the more involved situation of the periodic geometry of journal bearings; we recall that the Elrod–Adams method was first applied to these in [25]. Later on, also dynamically loaded bearings were considered on the basis of the JFO theory as the ADI method inherently favours the treatment of a real time-dependent lubrication problem, see e.g. [34]; for the numerical treatment of the thermal problem including cavitation we refer to [35].

In contrast to the approach by ADI, we modify the Elrod–Adams scheme in terms of an iterative technique aiming at directly solving the steady-state problem for virtually incompressible flow by employing a new technique of "annealing" with Ξ being the annealing parameter. The two main ingredients are as follows.

- We specify an artificial P_R-S-relationship rather than the physically motivated one having a fixed compliance Ξ^{-1} and here reading $P_R - P_C = \Xi \ln S$, adopted in [22, 24, 32] (note also its linear counterpart put forward by [33]), so as to effectively reduce the compressibility to a desired level by increasing Ξ.

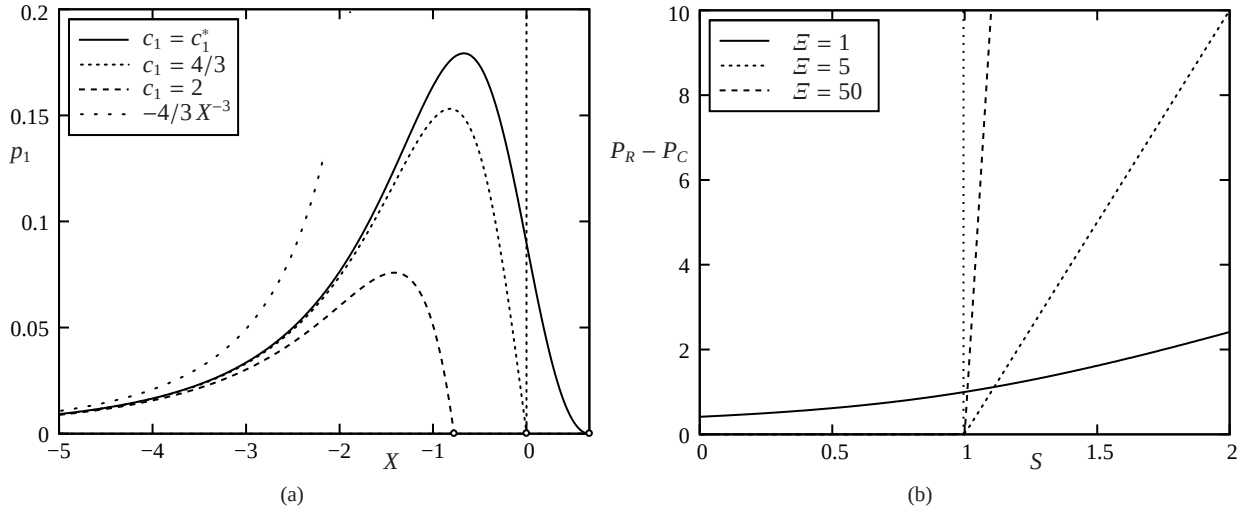

Figure 3: (a) shape of pressure spike p_1 for various values of c_1 (abscissa bounds X^* are indicated by circles) and leading-order asymptote by (A.5), (b) $P_R - P_C$ vs. S for various values of Ξ by (22) (in the second limit stated in (23) the dotted line indicating $S \equiv 1$ is approached).

- Stability and speed of the computations prove to be enhanced by setting $S = 1$ on the left-hand side of (11) right from the start of the iteration if the "incompressible" limit $\Xi \to \infty$ is targeted (as it is the case here).

We specifically take $P_R - P_C$ as positive throughout and allow it to take on arbitrarily large positive value outside the cavitation region, here defined by $S \leq 1$, by the suitable choice

$$P_R - P_C = \sqrt{1/\Xi^m + \Xi^2 (S-1)^{2n_o}} + \Xi (S-1)^{n_o}, \quad m \geq 4, \quad n_o = 1, 3, 5, \ldots . \tag{22}$$

Thus, a"smudge" or penalty function of $O(\Xi^{-m/2})$ depending on $1 - S$ of $O(\Xi^{-(m+2)/(2n_o)})$ describes $P_R - P_C$ as $\Xi \to \infty$:

$$P_R - P_C \sim \Xi^{-m-2} (1-S)^{-2n_o}/2 : \quad 1 - S \gg \Xi^{-(m+2)/(2n_o)}, \quad \partial P_R / \partial S \sim 2 n_o \Xi (S-1)^{n_o - 1} : \quad S - 1 \gg \Xi^{-(m+2)/(2n_o)} . \tag{23}$$

Satisfactorily good experiences in terms of robustness of the scheme were made by choosing $m = 4$ and $n_o = 1$ in (22). Larger values increase the speed of convergence towards the solution in the incompressible limit but also render the occurrence of instabilities in the iteration process more likely; so here the last word on an optimal choice is yet to be written. The resulting dependence of $P_R - P_C$ on S for different values of Ξ is illustrated in Fig. 3(b). Furthermore, we advantageously consider Ξ as a monotonically increasing function of the respective iteration step, i. Numerical experiments demonstrated that the particular choice $\Xi = \Xi_{min} + (\Xi_{max} - \Xi_{min}) \tanh[(0.04\,(i-1)]$ favours a rather fast rate of convergence. Limiting the increase of Ξ from Ξ_{min} by Ξ_{max} chosen as about 6–8 and 30, respectively, turns out to be necessary as it stabilises the growth of the oscillations observed near steep spatial gradients of S at the line of symmetry ($z = 0$) and close to the phase interface, where they are associated with spontaneous recondensation.

Let the i-th iterated approximations for S, P_R, and P_D be indicated by subscripts as follows. We initiate the iteration procedure by identifying $P_{L,1}$ formally with S_1 in (11) and solving the resultant linear form of the Reynolds problem. Then the Darcy problem is solved, yielding $P_{S,1}$ and thus a value for $v_{D,r}$. Together with S_1, this in turn feeds into (11). The iteration loop starts from here on ($i = 1$) and switches between solving the Reynolds and the Darcy problem: for this purpose, the Reynolds equation (11) is linearised about $S = S_i$ as enabled by (22) in order to be solved for an incrementally updated approximation S_{i+1}. This yields $P_{L,i+1}$ by (22), then the repeated solution of the Darcy problem gives $P_{S,i+1}$, and i is increased by 1. (A repeated toggling between sequenced solutions of the Darcy and the Reynolds problems at step i turned out to decelerate the speed of convergence.) We adopt a convergence criterion well-established for a technique as the present one that is aligned with the Newton–Raphson method to solve (sparse large-scale) systems of algebraic equations. It is based on the solution obtained in two consecutive iteration steps rather than the residuals formed by the original nonlinear system: convergence is reached if $\|P_{L,i+1} - P_{L,i}\|_2 < \sqrt{\epsilon}\,\|P_{L,i+1}\|_2$ where ϵ is the machine epsilon (for double-precision floating-point arithmetics about 5×10^{-16}) and $\|\cdots\|_2$ indicates

Table 2: Values of physical quantities used as input: note ambient pressure $\tilde{p}_a$, absolute vapour pressure $\tilde{p}_c + \tilde{p}_a$, reference pressure $\tilde{p}_{ref}$ by (9).

$\tilde{c}$ [mm]	$\tilde{r}_2$ [mm]	$\tilde{l}$ [mm]	$\tilde{\lambda}$ [mm]	$\tilde{\Phi}$ [mm²]	$\tilde{\Omega}$ [r.p.m.]	$\tilde{\eta}$ [Pa s]	$\tilde{p}_a$ [bar]	$\tilde{p}_c + \tilde{p}_a$ [Pa]	$\tilde{p}_{ref}$ [bar]
8.0×10^{-3}	4.0	11.0	3.75	1.8×10^{-9}	2000	0.0693	1.0	10^{-3}	$\doteq 217.71$

Table 3: Standard input parameters.

Γ	Λ	P_C	K
$\doteq 0.5289$	0.9375	$\doteq -4.593 \times 10^{-3}$	$K_s := 0.16875$

the Euclidian norm. Other definitions of the incremental error, also based on different norms, can be considered also. However, the criterion chosen proves advantageous as it is sufficiently sensitive to the intrinsically small variations of P_R in the cavitation region and, at the same time, yields most accurate results by avoiding difficulties in the convergence due to round-off errors. (For instance, from the triangle and norm inequalities one infers that replacing the normed difference adopted here by the difference of norms $\|P_{L,i+1}\|_2 - \|P_{L,i}\|_2$ or employing the also often used maximum norm, respectively, would lead to weaker criterions). Convergence is facilitated if under-relaxation is employed according to

$$(1-\omega)[S, P_R]_{i-1} + \omega[S, P_R]_i \mapsto [S, P_R]_i\,, \quad 0 < \omega < 1 \tag{24}$$

(no/over-relaxation with $\omega \geq 1$ did not work). That is, only the fractions ω of the updated approximations S_i and $P_{L,i}$ feed into the discretised Reynolds problem, to be solved for the consecutive update S_{i+1}, and the convergence criterion, respectively. An optimum implementation of the numerical scheme in terms of both robustness and convergence speed requires ω to take on the largest value that still entails a stable iteration for all the parameter constellations considered; in this respect $\omega \doteq 0.95 \div 0.99$ turned out to be a good choice. Abandoning such a very weak relaxation by setting $\omega = 1$, however, rendered the iteration unstable in some, albeit rare, cases.

We account for the sparsity of the matrices governing the discretised two linear subproblems by employing an adequate iterative canned solver invoking an appropriate preconditioner. Suitably spaced different meshes are used in the discretisations of the Darcy and the Reynolds problem: For the first an equidistantly spaced mesh formed by $20 \times 40 \times 30$ grid points in the r-, θ-, and z-directions, for the second one having 200×160 points in the θ- and z-directions, respectively, was used. The interpolation between these grids when the coupling conditions (17) are invoked is accomplished in an optimised manner by cubic splines. Near the phase interface an increased number of grid points is recommended to resolve the development of the discontinuity in S sufficiently accurate and avoid associated numerical difficulties. A solution-adaptive mesh refinement in the original (r,z)-space in that region, taking into account the varying cavitation boundaries, was implemented; more advanced strategies are currently scrutinised.

The results of the strategy outlined above are presented next. Some words to be left on the necessity of such an iterative scheme, which might address only the more mathematically interested reader, are postponed to the Appendix B.

4.2. Results — numerical simulations

As an example, we present the results of the calculation for a bearing with the geometrical parameters, rotational shaft speed $\tilde{\Omega}$, and lubricant properties displayed in Table 2. Also, we assume isotropy and homogeneity in Darcy's law (2). The corresponding value of the global (scalar) permeability $\tilde{\Phi} \equiv \tilde{\Phi}_{ref}$ results from adjusting measured and calculated values of the overall pressure drops of a flow of pressurised air through the annular seat in radially outward direction, i.e. from $\tilde{r} = \tilde{r}_1$ to $\tilde{r} = \tilde{r}_1 + \tilde{\lambda}$. We obtained these data by a homegrown experimental set-up and application of Darcy's law to compressible flow undergoing a quasi-static isothermal change of state. The values of $\tilde{\eta}$ and $\tilde{p}_c$ correspond to the measured properties of an ionic liquid used as lubricant. Non-dimensionalisation of the input values according to the parameters given in Table 1 yields the numbers shown in Table 3, with the coupling parameter K taking on its standard value K_s. Typically, the value of $|P_C|$ is very small. In the following, these values are kept fixed apart from the most essential system parameters ε and K.

In a first survey we varied ε as K takes on the value K_s. Figures 4, 5 display the solutions for the pressure and saturation for two distinct values of ε, namely, $\varepsilon = 0.1$ and $\varepsilon = 0.6$. Here P_R and S and thus the cavitation boundary results from interpolation of their data at the grid points. The minimum film thicknesses at $\theta = \pi$ obtained for these cases, see (10), are 9 μm and 4 μm, respectively. Cavitation commences shortly downstream of this location and develops in both the circumferential and the axial direction. The increase of the imposed load $\tilde{L}$, i.e. of ε towards 1, is reflected essentially by the following four observations:

(A) P_R exhibits a more abrupt change to the value of P_C,
(B) S takes on considerably smaller values,
(C) the cavitation boundary extends more closely to the edge of the bearing, $z = 1$, in agreement with the picture for ε close to 1 presented in Section Appendix A.3, and,
(D) characterised by the position of spontaneous recondensation in the area slightly upstream of $\theta = 2\pi$, it moves closer to this boundary from downstream.

A local discontinuity or an at least more-or-less pronounced sharp rise of S, associated with issue (D), is recorded for all the values of ε and K yielding converged solutions, in perfect support of our theoretical considerations in Section Appendix A.5 for $K = 0$, at the least. We note that saturation secludes the regime of cavitation from downstream in terms of a sudden jump even for any other parameter combination where convergence was achieved. On the basis of the present numerical results, this recurrent event can thus be safely considered as inevitable. The observations (A)–(D) also agree with the findings discussed in Section Appendix A.3. The question concerning the existence of the solutions and a threshold $\varepsilon^* < 1$ raised there is tied in with a likewise interesting one, namely, whether the recondensation front reaches $\theta = 2\pi$ for some value of ε below 1 or only finally in the limit $\varepsilon \to 1_-$. Currently, solutions are obtained only up to a value of ε situated near 0.9 (depending on the actual grid resolution and other numerical parameters affecting the convergence behaviour) as by exceeding this value slightly we encounter a failure of convergence. This patently points to the existence of such a threshold ε^* but the last word is not spoken yet.

In addition, we performed a parameter study where we vary gradually both the key quantities ε and K. The ranges of their values were chosen so as to achieve the clearly visible separation of the curves along which they are held constant: see Figs. 6–8. Herein the data indicated by the markers represent the results of the numerical study, interpolated smoothly by cubic splines. The only exception is the polar diagram showing the variation of the attitude angle Ψ in Fig. 6(b), where the markers are omitted as a much denser set of data points was used for generating sufficiently smooth curves. The split of the plots into parts (a) and (b) in Figs. 7 and 8 targets at enhancing their visible resolution in terms of the ranges of the respective parameters forming the abscissae.

Table 4 displays the calculated values of the bearing load capacity or, equivalently, the Sommerfeld number *So* for the (otherwise fixed) configurations represented by the values in Table 3. The associated variation of *So* is also plotted in Fig. 6(a). Rather unsurprisingly, the load capacity generally decreases for increasing values of K, where the impact of its variation on the load is more pronounced for lower values of K and medium to high values of ε. The values of K are chosen such that the load capacity approximately doubles for the most sensitive case $K = K_s$. Finally, as K becomes quite large, the bearing loses its capacity of carrying the load, in agreement with the considerations put forward in Section Appendix A.6. From Fig. 6(b), one detects how changing the value of K affects Ψ in dependence of ε, varied between 0 and the aforementioned threshold below which converged solutions were found. The (expected) range $\pi < \Psi \leq 3\pi/2$ reflects the occurrence of the pressure maximum and of cavitation in the, respectively, convergent ($0 < \theta < \pi$) and divergent ($\pi < \theta < 2\pi$) parts of the bearing. In the case of an almost solid bearing ($K = 0.001$), Ψ exhibits a major change when ε is varied in its entire range, bounded by 0 and 1. We remark that for more porous bearings, this change is not so drastic, and the curve globally flattens. On the contrary, Ψ attains smaller values the smaller K is in the limit $\varepsilon \to 0$, though we concede that the then intersecting curves can locally be hardly distinguished from each other. Eventually, the analysis leading to (A.3) gives $\Psi = 3\pi/2$ for $K = 0$ as $\varepsilon \to 0$.

In order to characterise the frictional behaviour, we plot the coefficient of friction μ versus the same parameters, ε and K, resolved into two regions, $0 < \varepsilon \leq 0.1$ and $0.1 \leq \varepsilon < 1$: see Fig. 7. The first-order pole at $\varepsilon = 0$ recognised in Fig. 7 is again predicted by the analysis in Section Appendix A.3. For fixed values of ε, the friction coefficient μ is seen to increase almost linearly when K is increased, at an almost constant slope for a fixed value of ε: see Fig. 8. Interestingly, varying the coupling parameter has comparatively little effect on the variation of μ. It is conceded, however, that the values of K used in our numerical calculations are only insufficiently large to verify the increase of μ in the form predicted by the asymptotic analysis in Section Appendix A.6 with satisfactory accuracy. For relatively high values of K and ε, the friction coefficient exhibits a slight increase by increasing ε, in contrast with

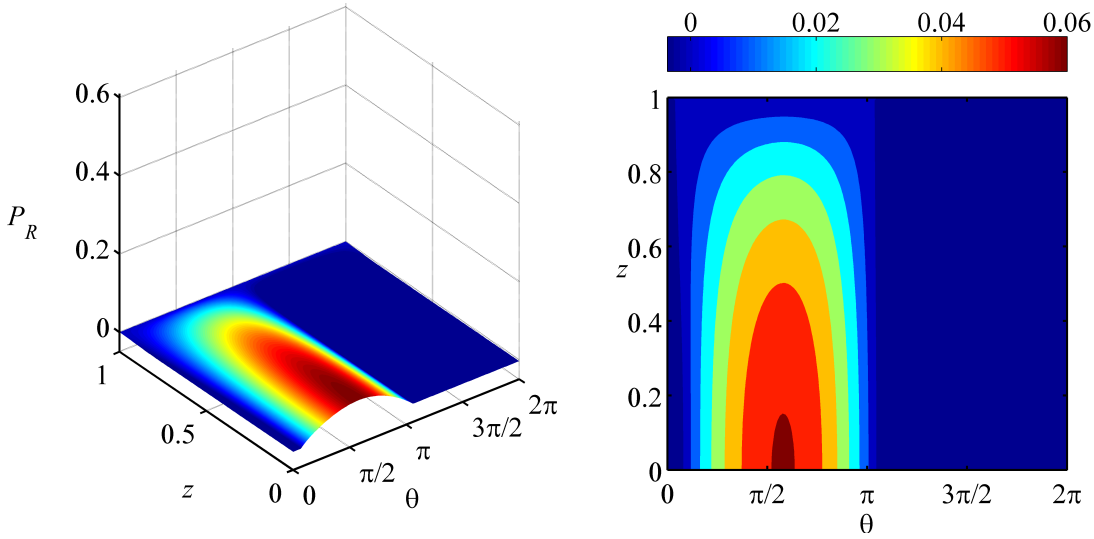

(a)

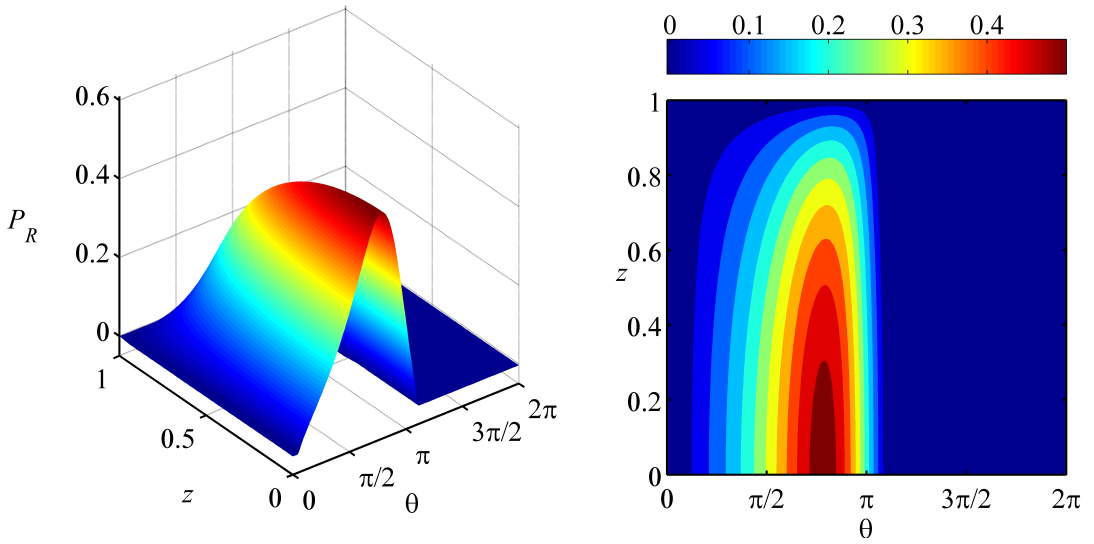

(b)

Figure 4: Pressure P_R in the lubrication gap for (a) $\varepsilon = 0.1$, (b) $\varepsilon = 0.6$.

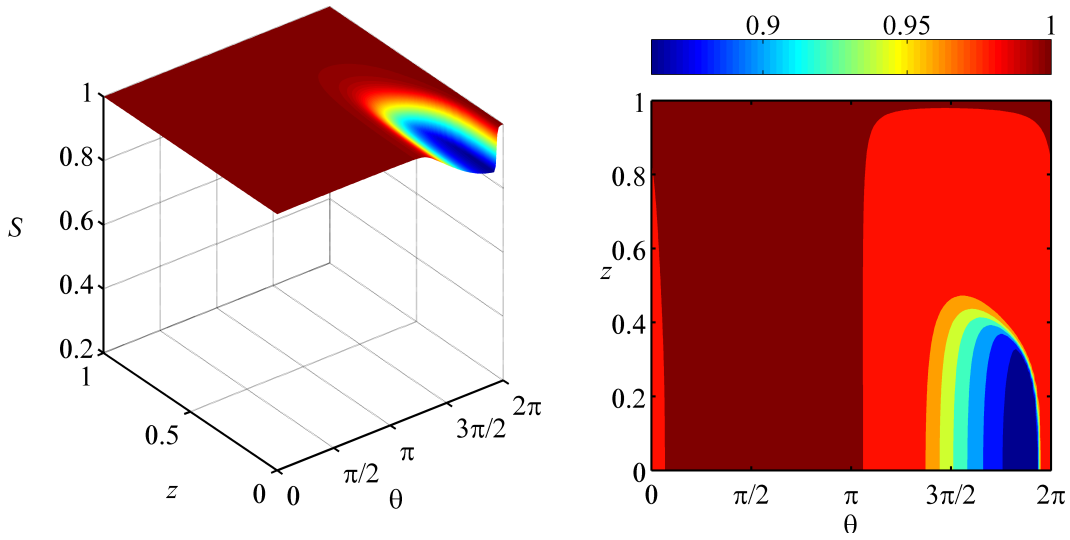

(a)

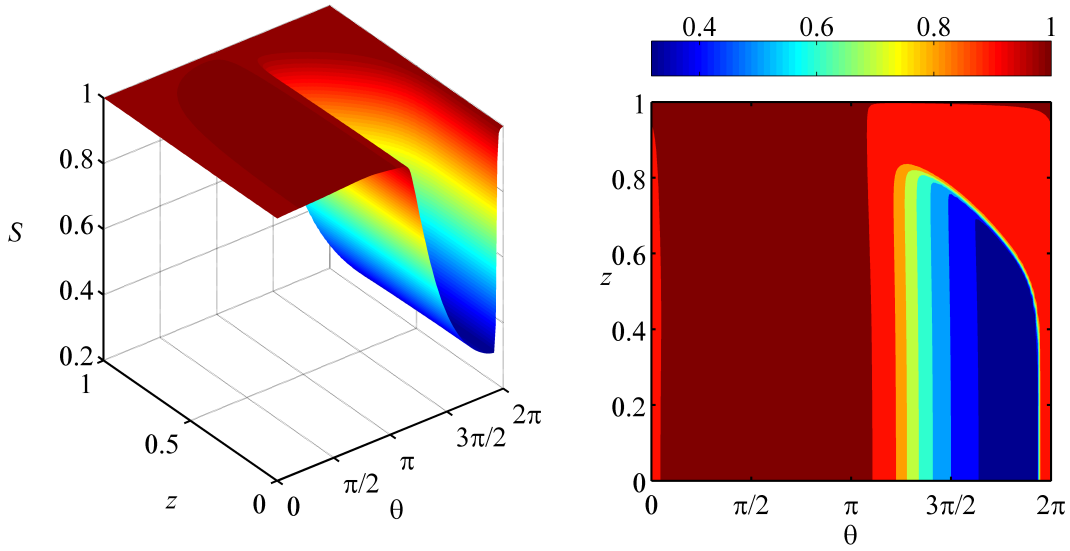

(b)

Figure 5: Saturation S in the lubrication gap for (a) $\varepsilon = 0.1$, (b) $\varepsilon = 0.6$.

Table 4: Rounded values of the Sommerfeld number *So* (bearing load $\tilde{L}$ [N]) for the standard values of Γ, Λ, P_C given in Table 3 and variable ε, K.

ε	$K_s = 0.16875$	$K = 0.4$	$K = 0.6$	$K = 1$	$K = 1.2$
0.1	0.0845 (51.56)	0.0791 (48.28)	0.0755 (46.06)	0.0695 (42.39)	0.0670 (40.87)
0.2	0.1529 (93.31)	0.1413 (86.25)	0.1337 (81.58)	0.1213 (74.06)	0.1163 (70.97)
0.3	0.2279 (139.09)	0.2075 (126.63)	0.1945 (118.72)	0.1743 (106.37)	0.1662 (101.43)
0.4	0.3159 (192.83)	0.2816 (171.89)	0.2610 (159.31)	0.2303 (140.59)	0.2185 (133.36)
0.5	0.4252 (259.55)	0.3676 (224.37)	0.3356 (204.87)	0.2910 (177.62)	0.2744 (167.51)
0.6	0.5675 (346.43)	0.4695 (286.57)	0.4210 (256.96)	0.3578 (218.41)	0.3355 (204.78)
0.7	0.7595 (436.58)	0.5920 (361.44)	0.5205 (317.71)	0.4339 (264.88)	0.4047 (247.06)
0.8	1.0212 (623.34)	0.7448 (454.66)	0.6429 (392.47)	0.5278 (322.15)	0.4905 (299.41)

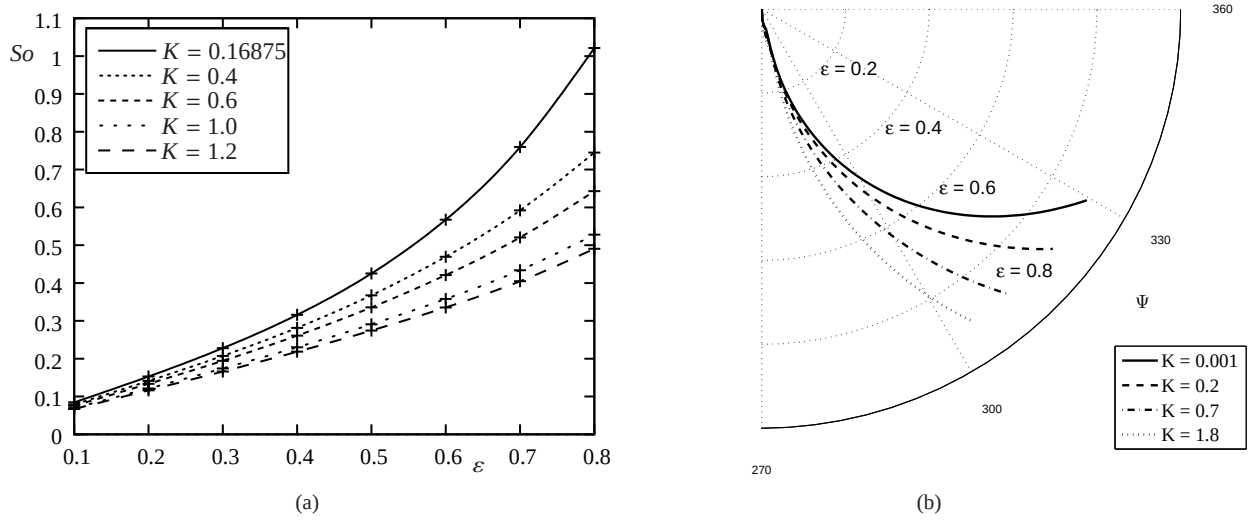

Figure 6: (a) Sommerfeld number *So* and (b) attitude angle Ψ [deg] vs. eccentricity ratio ε for various values of the permeability parameter K.

the overall decreasing trend. This regime is of particular interest and subject to further investigations in the context of the existence of the aforementioned threshold $\varepsilon^* < 1$.

4.3. Results — comparison with experiments

The study is completed by the presentation of some preliminary experimental results, serving as a starting point for a doubtless needful more elaborate validation of the proposed theoretical model and its numerical predictions.

From a traditional engineering point of view, an overview on the behaviour of journal bearings under the different conditions of lubrication (from mixed to fully hydrodynamic) is provided by plotting the friction coefficient μ versus the rotational speed $\tilde{\Omega}$ for constant values of the applied bearing load $\tilde{L}$, i.e. in terms of the celebrated Stribeck curves. Here only their fully hydrodynamic branch is of interest. In practice, the data required for such a plot are obviously quite accessible through adequately designed experiments but cannot be extracted directly from those obtained by simulations: the latter are primarily parametrised by the varying eccentricity ratio ε, which, however, is incapable of measurements by our experimental setup, rather than $\tilde{L}$. Hence, correlating the data presented in Section 4.2 to experimentally obtained ones requires their interpolation in terms of $\tilde{L}$ rather than ε by an advanced strategy that masters the inversion of *So* given as a function of ε according to (19). To this end, smooth cubic-spline interpolation was adopted to represent the functional dependences of *So* and μ_n on all the five parameters by fitting to their values used in both the experiments and the numerical calculations. Here the variation of the kinematic viscosity $\nu := \tilde{\eta}/\tilde{\rho}_l$ with temperature is implemented numerically on the basis of the classical empirical Ubbelohde–Walther formula:

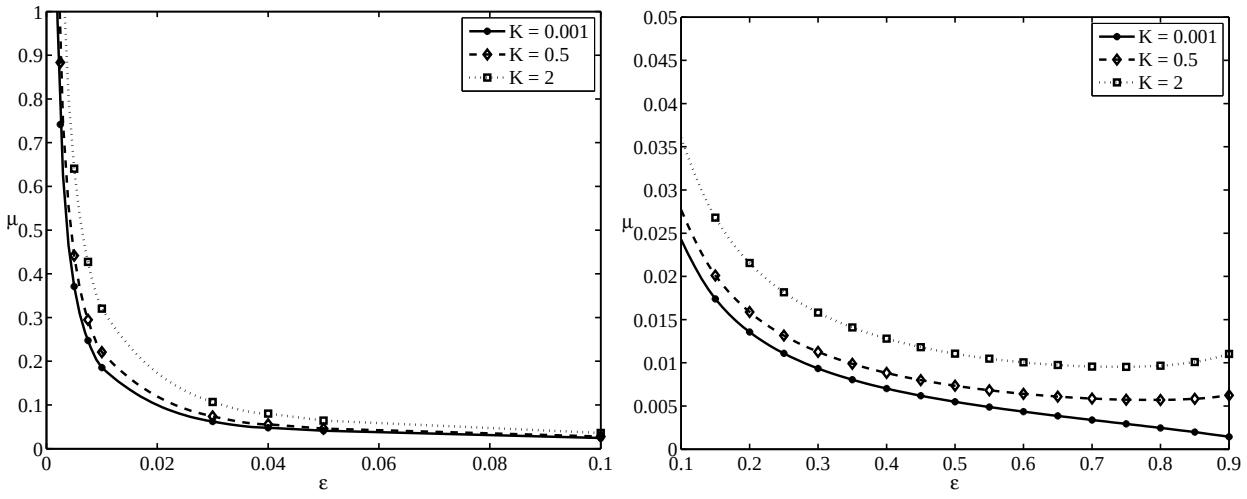

Figure 7: Friction coefficient μ vs. eccentricity ratio ε for various values of the permeability parameter K.

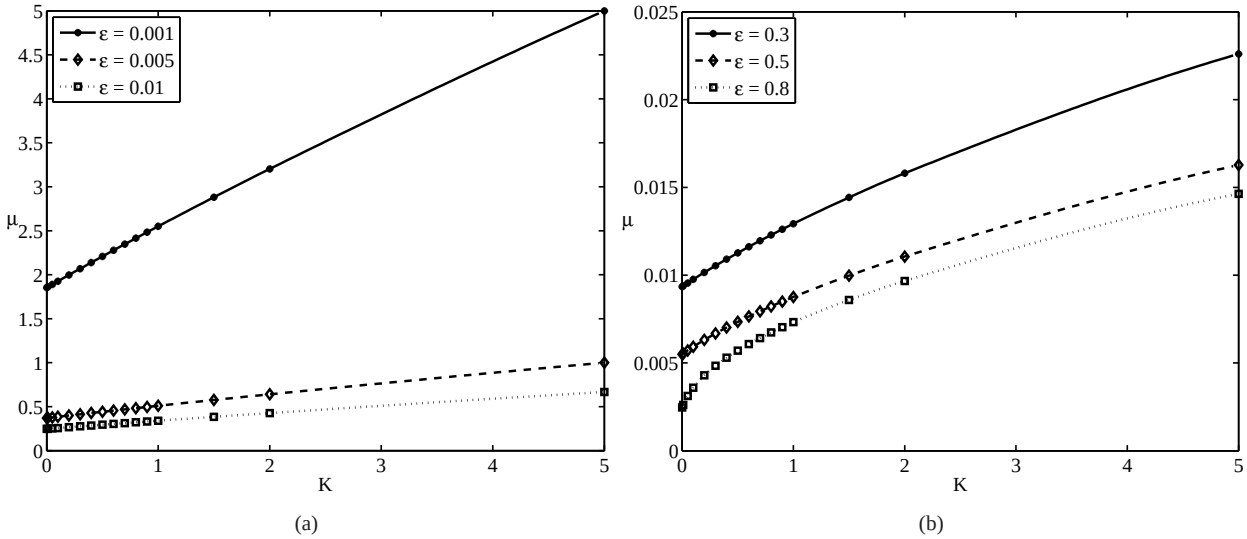

Figure 8: Friction coefficient μ vs. coupling parameter K for various values of the eccentricity ratio ε.

$\lg\lg(\nu + \tilde{f}) = \tilde{a} - \tilde{b}\lg\tilde{T}$ involving ν [mm²/s], the absolute temperature $\tilde{T}$ [K] of the lubricant, lubricant-specific constants $\tilde{a}$ and $\tilde{b}$, and a correction factor $\tilde{f}$ ($\tilde{f} \doteq 0.7$–0.8 for mineral oils). Let us finally emphasise that a comparison between experimental and numerical data requires a satisfactory (long-term) running-in of the bearing in the regime of fully hydrodynamic lubrication.

The experiments were carried out on sintered bearings with the geometrical parameters specified in Section 4.2, but with varying porosities, 20% and 25%, combined with two values of the supplied load: 10 N and 100 N. The casing weight adds up to the total load, such that the corresponding specific pressures are 0.5 N/mm², and 1.5 N/mm². Standard Stribeck tests involve both an acceleration regime as well as a deceleration one, where the rotational speed is varied gradually. The profiles are: 0–600 r.p.m. in 50 s, 600–3000 r.p.m. in 90 s, a constant regime at 3000 r.p.m. for 25 s, followed by a similar profile for a subsequent deceleration sweep. The measured temperature of the lubricant exhibits a slight monotonic dependence on the speed. For the reason stated at the end of last paragraph, merely the results obtained during acceleration of the shaft rotation are used for the comparison. Three ionic liquids (ILx) with different viscosity grades (VGy) were chosen as lubricants: IL1 (VG32), IL2 (VG150), IL3 (VG220). Here the second one is a binary volumetric 1:1-mixture of the other two each of which consists of just one salt component.

We discuss all four configurations of interest on the basis of the results shown in Figs. 9. The bold curves represent the output of a low-pass Gaussian filter applied to the raw measured data. Accordingly, the thin lines connecting these original data points are subject to pronounced oscillations indicating deviations from perfect steady-state conditions in the experimental set-up. The curves referring to the simulations arise from smooth cubic-spline interpolation of the markers indicating the data obtained numerically. It appears that the best correlation between experiments and calculations is observed in the case of lightly loaded bearings: Figs. 9(a,c,e). On the other hand, for quite high loads, the discrepancy between the two sets of data is accentuated: Figs. 9(b,d,f). The numerical results for a prescribed load confirm the findings inferred from (19), (20), (21) and (9) that the Sommerfeld number So decreases but the friction force and, hence, the coefficient of friction μ increase (almost linearly) when the rotational speed $\tilde{\Omega}$ increases: note that μ decreases at a constant value of the latter for an increasing eccentricity ε. The absence of data points in some regimes is due to the failure of the numerical interpolation scheme which for the given parameters yields values corresponding to the mixed lubrication domain. Nevertheless, at least for relatively low loads promising agreement is spotted, and the trends of the computed curves matches those of the measured ones satisfactorily well throughout. The apparent offset is most likely due to the serious uncertainty regarding the value of the permeability used in the simulations and/or non-Newtonian effects. Concerning the role of the porosity in the frictional behaviour, a general rule cannot be deduced from the rather small range of porosities available: the variation from 20% to 25% shows no notable impact on μ. Note that Figs. 9(c,d) display the effect of mixing the lubricants used in the cases (a,b) and (e,f).

Complete geometrical similarity between different bearings means equal values of Γ, Λ, and, as long as capillary effects are not considered, also of K. It can often be assumed within a set of individual bearings of the same type but different sizes with sufficient reliability. Due to the usually negligibly small variations of P_C, then So and μ_n depend essentially on ε solely. By eliminating this quantity, one ends up with the non-dimensional representation μ_n versus $1/So$ (proportional to the Gümbel–Hersey number) of the Stribeck relationship in the fully hydrodynamic regime, according to (19) and (9): see Figs. 10. Here only the data for the pure ionic liquids are used as their thermophysical properties ($\tilde{\eta}$, $\tilde{p}_c$) are available at a higher accuracy. The collapse of the data onto a single curve and a point in the (So, μ_n)-plane would indicate the conditions of complete geometrical and mechanical similarity, respectively. Therefore, future efforts in validation of the results of simulations include their careful evaluation by their representation in this particular form. As a consequence, the observed deviations of the measured data points from this universal relationship will serve as a measure to categorize the influence of additional effects, not yet considered in our investigations.

5. Concluding remarks and further outlook

A mass-preserving model of vaporisation cavitation in the context of sintered journal bearings is proposed and studied in terms of the reliability and consequences on a self-consistent description of the lubrication process theoretically, numerically, and, even if undeniably at a premature level, also experimentally. By the new numerical technique adopted, we solved iteratively the system of equations, essentially consisting of the Reynolds and Darcy equations supplemented with the Jakobsson–Floberg–Olsson condition for coping with the onset of cavitation and spontaneous recondensation, with very high accuracy at comparatively little computational time and effort as the method directly

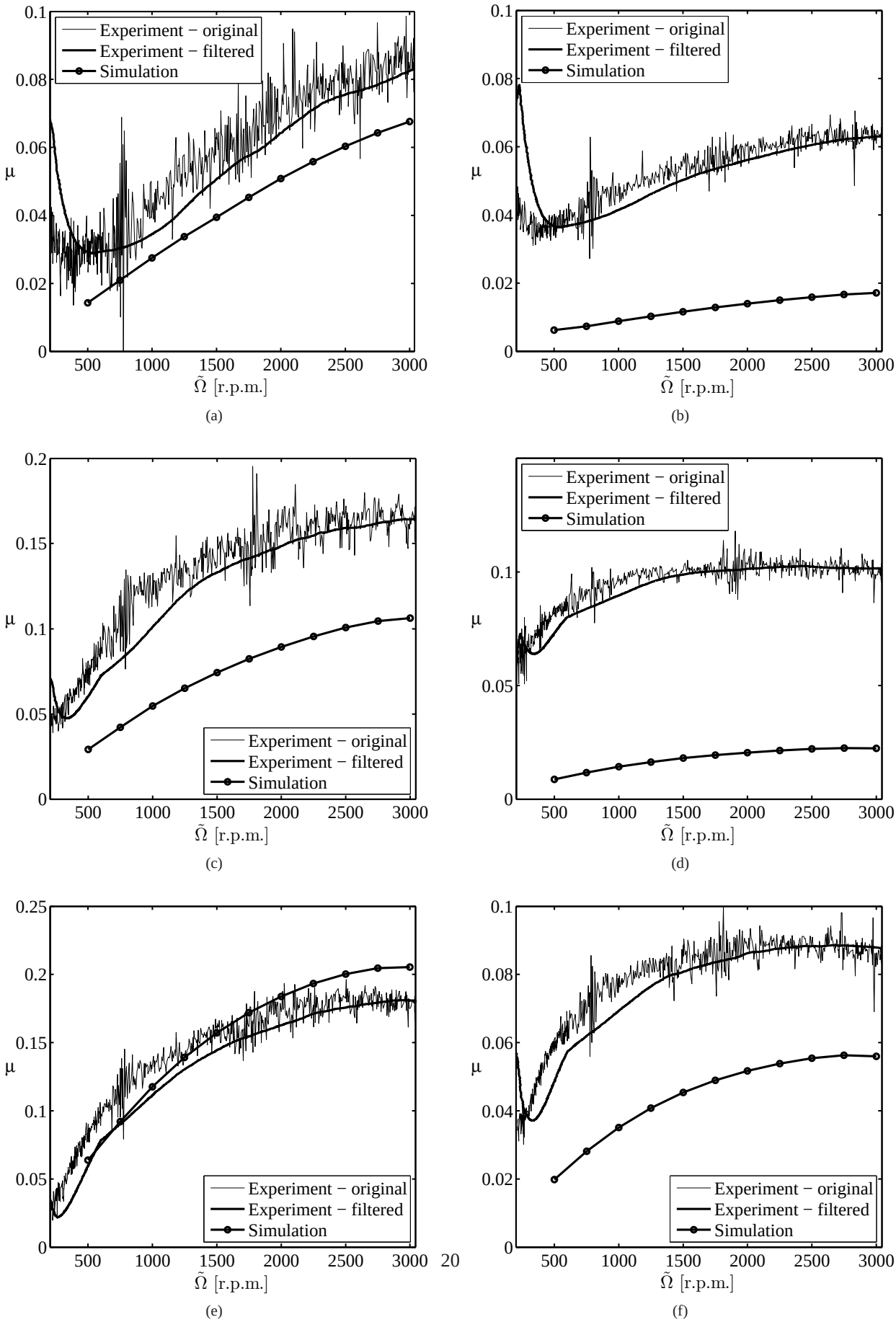

Figure 9: Data by experiments vs. by simulations for a bearing with a porosity of 20%, lubricated with IL1 (a,b), IL2 (c,d), IL3 (e,f), and under a shaft loading $\tilde{L}$ of 10 N (a,c,e), 100 N (b,d,f).

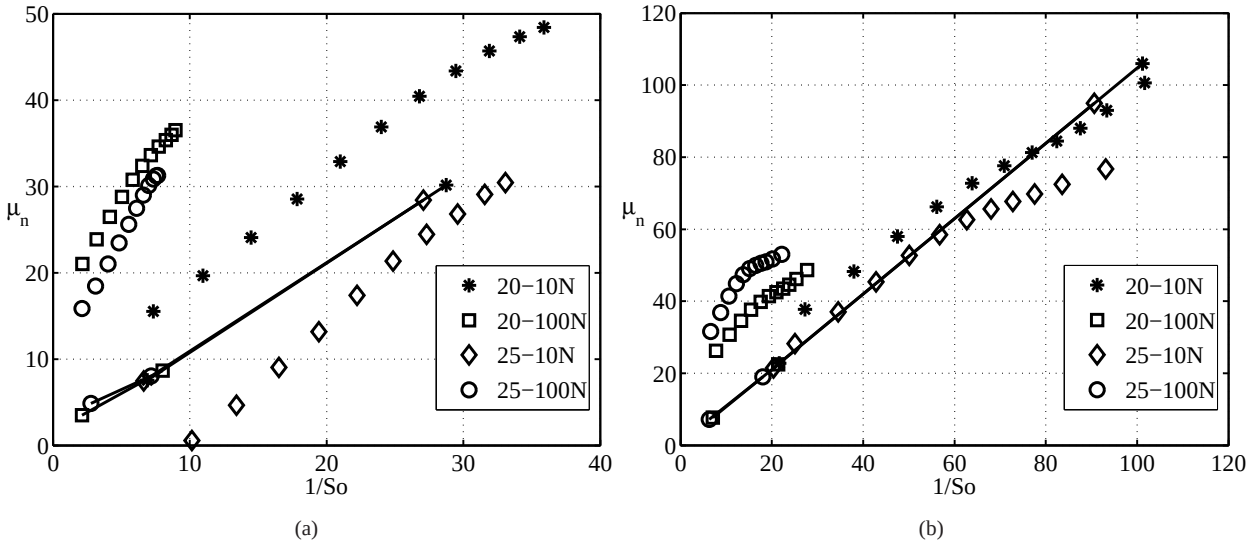

Figure 10: Normalised friction coefficient μ_n vs. $1/So$ for IL1 (a) and IL3 (b); experiments/simulations: markers without/with connecting straight lines.

aims at predicting the steady-state operation of the bearing in straightforward manner, in contrast to previous approaches. The main objective was to gain insight into the development of the lubrication pressure and saturation tied in with the phase changes taking place inside the lubrication gap. Considering the benefit for engineering applications, we believe that the — albeit showcase — numerical results offer encouraging perspectives into a successful improvement of existing tribological design of such bearings. In terms of the frictional behaviour, the comparison between calculated and measured values of the friction coefficient discloses some discrepancies, but nonetheless also a promising trend.

Among the current and future demands of research activities already outlined at the respective stages of this study, four tasks, viewed as primarily relevant, deserve to be highlighted as follows.

Measuring the phenomenon of cavitation in a sintered journal bearing is difficult and available data scarce, so the validation of results by simulations to some extent subject to physical intuition yet. From this point of view, the numerical study carried out in this work shows that the proposed model predicts satisfactorily well the phenomenon of cavitation for wide and feasible ranges of the varied key quantities in the space of the (five) dimensionless groups involved, namely the eccentricity ratio ε and the permeability parameter K. However, it appears that there exists a certain threshold for ε for any fixed value of K beyond which converged solutions of the lubrication problem describing stationary bearing operation cannot be achieved. Hence, the first task arises quite naturally: perturbation methods along with homogenisation techniques can constitute the basis of future efforts meant to either numerically determine the associated boundaries in the parameter space that confine the regimes where solutions exist or stabilise these in case their existence can be guaranteed for all values of ε exceeding this threshold, even in the limit $\varepsilon \to 1_-$. In particular, K is required to take on positive values in order to allow for the regularisation of the otherwise unbounded growth of the pressure spike near the position of minimum fluid film thickness, where the distinguished limit $K \to 0$ as $\varepsilon \to 1_-$ poses the central problem currently under investigation. Eventually, microscopic effects due to surface roughness and porosity then come into play at leading order and, therefore, have to be accounted for in a rigorous extension of the current theory.

The second issue is associated with the saturation jump as one of the most notable predictions of the proposed flow description. Here the need for an elaborate effort both analytically and numerically is apparent in order to settle the intriguing question whether the discontinuities remain or are smoothed out for finite values of K. Specifically, the thorough investigation of rather weak jumps, associated with infinitesimally small cavitation regions, being the distinguishing mark of certain parameter configurations and, in the present study, of lubricant flow referred to as a marginally cavitating one, is expected to shed light on the internal structure of the flow, which is of high interest even

if described still within the framework of classical lubrication theory.

In the latter context the third question of utmost importance is raised, namely, which interfacial physical effects, not addressed in the present study, have to be taken into account consistently in this regularisation process when the thickness of the resulting layer encompassing the cavitation boundary becomes correspondingly small as $K \to 0$: there lubrication theory in the form adopted here needs to be modified and extended accordingly.

Finally, the fourth subject presently under investigation concerns the application of the homogenisation process to the Reynolds problem, which then completes the self-consistent flow description of the two- (micro- and macro-) or multi-scale approach.

In addition to the more severe shortcomings of the current theoretical approach and associated topics of research addressed above, it lacks, amongst other physical aspects of rather minor interest, the inclusion of non-Newtonian behaviour of the lubricant and a sufficiently reliable prediction of the permeability in dependence of the measured porosity. Resolving these issues would also contribute substantially to an improved model of cavitation. Unsteady operating conditions and/in combination with capillary effects represent further challenges worth to be met.

Notwithstanding the undeniably tremendous progress made towards a comprehensive understanding of the lubricant flow through self-lubricated journal bearings in the last decades and considering the vast amount of literature on this subject, we believe the present work clarifies some of the hitherto unresolved aspects of (vaporisation) cavitation in such devices. Without doubt, much more has to be done in this direction not only analytically/numerically but also in terms of an experimental validation. This will certainly create added value for theoreticians as well as practitioners.

Acknowledgements

The authors would like to acknowledge the financial support of this research by the FP7 Marie Curie Actions Training Network *MINILUBES* and the Austrian Research Promotion Agency (FFG; grant no.: 824187, project acronym: *XTribology*). It was carried out at the *Excellence Center of Tribology* at AC²T research GmbH. Also, we like to thank Dr. Stefan Eder (AC²T research GmbH) for exceptional discussions about the coding of the numerical scheme and his support regarding its implementation and the reviewers for their helpful comments. Special thanks go to GKN Sinter Metals S.P.A. (Bruneck, Italy) for providing the authors with data referring to real (manufactured) bearings and supply of and technical assistance with an experimental rig.

Appendix A. Theoretical aspects

In the following, we outline the six points as raised in Section 3: Sections A.1–A.6.

Appendix A.1. Cavitation-free sinter flow

The formulation of (10)–(17) is self-consistent insofar as $P_D > P_C$ is found for $1 < r < 1 + \Lambda$ — otherwise a gaseous phase would also take place in the seat and the application of Darcy's law (2) and the adopted interpretation of $v_{D,r}$ obviously be in doubt. However, we now prove by considering smooth solutions of (15) in that region subject to (16) that the above inequality is satisfied inside the seat and P_D is equal to P_C possibly only at its boundary $r = 1$; cf. a related comment in [25].

Proof. Equation (15) is elliptic as the permeability components $\Phi_{r,\theta,z}$ are positive, so that P_D assumes its extremal values at the outer boundary $r = 1 + \Lambda$ and/or in the limit $r \to 1$ towards the inner boundary of the toroidal computational domain that describes the sinter (which just restates the solenoidality of the velocity of the lubricant). That is, the solution P_D exhibits neither closed inner regions nor such confined by one of these boundaries where $P_D < P_C$. As the only remaining possibility, such a region forms a single-connected tube that extends from the inner to the outer boundary and the facing sides $z := \pm 1$ of the torus. Then $P_D = P_C$ on the generated surfaces of the tube and its intersection with the inner boundary. Consequently, the normal gradients of P_D at these bounding areas directed outwards of the tube are positive throughout. Since they vanish identically at its intersection with the outer boundary by (16), the values of P_D must take on a local minimum smaller than P_C inside that tube. However, this contradicts the introductory statement and hence confirms that the occurrence of cavitation is restricted to the lubrication gap.

Appendix A.2. Mass deficit of active lubricant in loaded bearing

Insulation of a fully submerged bearing exhibiting complete impregnation by an incompressible liquid lubricant has an interesting side effect. The sinter is always soaked by the same amount of lubricant, independent of the specific operating condition described by certain values of the parameters in Table 1. However, this is not necessarily true for the lubrication gap: its volume is invariant with respect to a variation of ε, but not so are its fraction where cavitation occurs, i.e. $S < 1$, and the specific distribution of S therein.

The resulting mass deficit relative to the total mass of lubricant in the bearing has a magnitude of the order of the principal approximation error given by (4). We then conveniently introduce the ratio ξ, $\tilde{\rho}_v/\tilde{\rho}_l < \xi \leq 1$, of the actual lubricant mass in the gap to the constant one if cavitation was absent,

$$\xi(\Gamma, \Lambda, P_C, \varepsilon, K) := \int_0^1 \int_0^{2\pi} H(\theta)\, S(\theta, z)\, \mathrm{d}\theta\, \mathrm{d}z \Big/ \int_0^1 \int_0^{2\pi} H(\theta)\, \mathrm{d}\theta\, \mathrm{d}z = \frac{1}{2\pi} \int_0^{2\pi} H(\theta) \int_0^1 S(\theta, z)\, \mathrm{d}z\, \mathrm{d}\theta\,. \quad \text{(A.1)}$$

According to (8), then the equivalent volume or mass fraction containing the fully liquid phase is calculated from

$$\frac{1}{2\pi} \int_0^1 \int_0^{2\pi} H(\theta)\, \alpha_l(\theta, z)\, \mathrm{d}\theta\, \mathrm{d}z = \frac{\xi - \tilde{\rho}_v/\tilde{\rho}_l}{1 - \tilde{\rho}_v/\tilde{\rho}_l}\,. \quad \text{(A.2)}$$

Varying the load in terms of *So* or, equivalently, ε as all other parameters in Table 1 are kept fixed allows for a most vivid interpretation of the mass defect in the lubrication gap. Then ξ accounts for the comparison of an unloaded bearing ($\varepsilon = 0$) with one where the applied load finally causes cavitation. Therefore, we have $\xi = 1$ for values of the load or ε below certain thresholds indicating marginal cavitation. As confirmed by the numerical study, see Section 4, ξ decreases if those quantities increase further. Under the assumption of an insulated bearing made in the present study, this mass deficit can be only unravelled by the presence of the liquid rings that seal the bearing ends, as already mentioned in Section 2.2, and very thin liquid films covering the outer surface of the seat, both serving as additional mass reservoirs: they apparently grow for an increasing load above the aforementioned critical value. This has to be confirmed in the course of a local analysis of the formation of these flow phenomena due to capillary and centrifugal forces.

Appendix A.3. Limits of lightly- and heavily-loaded bearings

We address some interesting aspects of the lubrication problem formulated in Section 2.2 for these two cases by asymptotic analysis.

Appendix A.3.1. Very light loading

The problem reflects the imposition of a sufficiently light bearing load $\tilde{L}$ in two different ways:

1. Operating conditions and lubricant properties affect $\tilde{p}_{ref}$ via $\tilde{\Omega}$ and $\tilde{\eta}$, see (9), and $\tilde{p}_c$. Under usual conditions, this gives numerically rather small values of P_C. However, $\tilde{p}_{ref}$ can be so small, primarily due to a correspondingly low rotational speed $\tilde{\Omega}$, so that $|P_C|$ assumes an appreciable magnitude which includes the possibility $P_C \ll -1$. But even in the — rather unconventional — latter case P_R admits a finite limit that appropriately resolves the correspondingly weak variations of $\tilde{p}$ without provoking nucleation of a vapor cavity (marginal cavitation): $S \equiv 1$. Accordingly, so do the eccentricity ratio ε and hence *So*, the complementary attitude angle $\Psi - 3\pi/2$, and μ_n as given by (20), (21). In Section 4.1 it will turn out that this pathologic case requires a separate numerical treatment (not addressed so far).
2. In contrast, one usually expects $|P_C| \ll 1$, in particular when novel promising lubricants as the ionic liquids mentioned in Section 2.1 are in use. Then the common notion of "lightly-loaded" applies, namely the limit of vanishing eccentricity, i.e. $\varepsilon \ll 1$ and an almost concentric gap by (10). This implies an expansion of the form $P_R \sim \varepsilon P_{R0}(\Gamma, \Lambda, P_C, K) + O(\varepsilon^2)$, but cavitation-free flow, i.e. $S \equiv 1$, occurs only for ε being sufficiently smaller than $|P_C|$. Accordingly, (20) and (21) then yield the Maclaurin expansion

$$[So/\varepsilon,\ \Psi,\ \varepsilon\mu_n] \sim [So_0,\ \Psi_0,\ \mu_{n0}]\,(\Gamma,\ \Lambda,\ K) + O(\varepsilon) \quad \text{with} \quad \Psi_0(\Gamma,\ \Lambda,\ 0) = 3\pi/2\,, \quad \mu_{n0} = 3\pi\tilde{c}/(\tilde{r}_2 So_0). \quad \text{(A.3)}$$

   Here the explicit expression for Ψ_0 arises from the familiar antisymmetry of P_R with respect to $\theta = \pi/2$ for a submerged massive bearing under the neglect of cavitation. Consequently, neglecting the contribution of the Poiseuille flow to μ_n yields the form of μ_{n0}. Also, well-known Petroff's law, cf. [36], pp. 483–484, is recovered by this asymptotic representation. We add that $I_C = \pi/(3\sqrt{1-\varepsilon^2}\,)$ if cavitation is neglected, i.e. $\alpha_l \equiv 1$ in (21).

Appendix A.3.2. Very heavy loading

We appropriately address the opposite case of a heavily-loaded bearing by considering the limit $\delta := 1 - \varepsilon \to 0$. For sufficiently small values of δ, this finally has to take into account the aforementioned microscopic effects of surface roughness and surface porosity in the leading-order modification of the Reynolds equation as the homogenisation process adopted ceases to be valid in a small vicinity of the position where the gap height H assumes its minimum, $\theta = \pi/2$. Specifically, these effects may become dominant in the region where $X := \sqrt{\delta}\,(\theta - \pi/2) = O(1)$ and (10) is rewritten as $H \sim \delta h_1(X) + O(\delta^2)$ with $h_1 := 1 + X^2/2$.

In case of a massive bearing, i.e. for $K = 0$, this yields singular inner and outer expansions of the lubrication pressure for, respectively,

$$X = O(1)\colon \quad P_R \sim \delta^{-3/2} p_1(X, z) + O(\delta^{-1/2})\,, \quad \theta - \pi = O(1)\colon \quad P_R \sim P_{R1}(\theta, z) + O(\delta)\,, \tag{A.4}$$

with rescaled pressure distributions p_1, P_{R1} of $O(1)$. Their match accomplishes the regularisation of a pressure spike near $\theta = \pi/2$ that grows beyond all bounds as $\delta \to 0$: from (11), we find that $P_{R1} \sim (4/3)(\pi - \theta)^{-3} + O[(\pi - \theta)^{-1}]$ in the limit $\theta \to \pi_-$, whereas P_{R1} has to be found numerically for $0 \le \theta < \pi$ and $\pi < \theta \le 2\pi$. Due to the disregard of the aforementioned effects, however, the function $p_1(X, z)$ is still governed by the correspondingly reduced form of (11), where we additionally set $S = 1$. Integrated once, this gives $h_1^3\,\partial p_1/\partial X = h_1 - c_1(z)$. It is the initially unknown coefficient c_1 that accounts for the regularisation and, by repeated integration over X from $X = -\infty$, for the match with P_{R1} in terms of the upstream built-up of the pressure peak. This finally gives the analytical solution

$$p_1(X, z) = [4 - 3c_1(z)]\left[\frac{X}{8h_1(X)} + \frac{\sqrt{2}}{8}\left(\arctan\left(\frac{X}{\sqrt{2}}\right) + \frac{\pi}{2}\right)\right] - \frac{c_1(z)X}{4h_1(X)^2} \;\sim\; \frac{4}{3(-X)^3} + O\left(X^{-5}\right) \;\text{ as }\; -X \to \infty\,. \tag{A.5}$$

Regarding the X-dependence of p_1, its deviation from its mean value is skew-symmetric. For $c_1 > 1$, p_1 attains the desired maximum and a minimum further downstream, at $X_\mp(c_1) := \mp\sqrt{2(c_1 - 1)}$. The minimum is positive/negative if c_1 is smaller/greater than a critical threshold $c_1^* \doteq 1.225763$, found by numerical evaluation of (A.5). Therefore, the match of p_1 with variations of P_R of $O(1)$ downstream of $\theta = \pi$ demands the existence of an asymptotically small flow region encompassing the location $X = X^*(c_1)$ defined by $p_1(X^*, z) = 0$ and $p_1(X, z) > 0$ if $X < X^*$. This in turn requires $c_1 \ge c_1^*$, and the aforementioned match is characterised by a zero or or negative gradient $(\partial P_1/\partial X)(X^*, z)$ for $c_1 = c_1^*$ with $X^* = X_\mp(c_1^*)$ or $c_1 > c_1^*$ with $X^* < X_+(c_1)$, respectively. For the resulting distribution of the positive values of p_1 (where $X \le X^*$) see Fig. 3(a). The maximum of p_1 decreases for increasing values of c_1. For $c_1 = 4/3$, (A.5) reduces to the classical algebraic pressure distribution for a gap of parabolic shape [10]. Needless to say, here the outer pressure function P_{R1} and c_1 depend parametrically on Γ, Λ, and P_C. The following leading-order results are immediately found from (20), (21) and the above analysis for

$$\left.\begin{aligned} K = 0\colon \quad & \left[\delta So,\, \mu_n/\sqrt{\delta}\right] \sim [So_1,\, \mu_{n1}]\,(\Gamma,\, \Lambda,\, P_C)\,, \quad \Psi \sim \pi \quad \text{with} \\ & [So_1,\, \mu_{n1}] = \int_0^1 \left[\int_{-\infty}^{X^*(c_1)} p_1(X, z)\,,\; \frac{1}{So_1}\int_{-\infty}^{X^*(c_1)} \left(\frac{2}{3h_1(X)} - \frac{c_1(z)}{2h_1^2(X)}\right) + \frac{1}{So_1}\int_{X^*(c_1)}^{\infty} \frac{S(\theta, z)}{6h_1(X)}\right] \mathrm{d}X\,\mathrm{d}z\,. \end{aligned}\right\} \tag{A.6}$$

One can easily express the integrals over X in closed forms.

It is noted that the physical meaning of the small flow region addressed above lies in the description of the inevitable onset of cavitation. However, the associated completion of a perturbation theory coping with the associated regularisation process in a self-consistent manner can not be guaranteed for the time being: a preliminary analysis aiming at continuing the description of cavitating flow further downstream and towards the edge of the bearing when viewed from a position where $0 < X^* - X = O(1)$ and values of $z > 0$ not too close to 1 points to some subtle difficulties. This procedure essentially yields the form of the coefficient function $c_1(z)$ and, hence, $X^*(c_1)$, as well as the variation of S in (A.6), which completes the flow description in the limit $\delta \to 0$ for $K = 0$. The detailed splitting of the flow in the limit defined by $K = 0$, $\varepsilon \to 1_-$ as $(\theta - \pi)^2/(\varepsilon + 1) = O(1)$ is subsumed as follows.

As a starting point of the analysis, one considers the core region defined by thin stripe $0 < X^* - X = O(1)$, $z \ge 0$, $1 - z \gg \sqrt{\delta}$ where (A.5) holds. The function $c_1(z)$ is determined by matching this core layer with the encompassing flow regions up- and downstream of it, and a small square edge region where $1 - z = O(\sqrt{\delta})$ such that the left-hand side of (11) is retained in full. In these regions (A.4) and (A.5) cease to be valid, and it is the last domain which

crucially accounts for the existence of a two-phase interface as cavitation cannot extend towards the bearing edge if $P_C < 0$, as assumed. Amongst others, then the following steps, here not given in all details, have to be performed: solving the leading-order lubrication problems arising in these small regions subject to matching conditions in all directions, then in the adjacent extended core region where $0 < X - X^* = O(1)$ and $P_R \sim P_C$ subject to the match with the main region further downstream where $P_R \sim P_{R1}$, see (A.4). This finally establishes the desired form of S in (A.6).

The current knowledge of the flow structure for a heavily-loaded, massive, insulated bearing can be condensed into the statement that the existence of solutions for all values of ε satisfying $0 \le \varepsilon < 1$ has to be doubted, at least for $K = 0$. At this stage the intriguing question arises whether solutions with $S > 0$ exist for all values of ε between 0 ($P_R \equiv P_D \equiv 0$) and 1 or just for $\varepsilon \le \varepsilon^* < 1$ where ε^* denotes a particular threshold. Its existence would point to the loss of steady-state operation of the bearing even at finite loads or, equivalently, for a finite value of *So*. On the other hand, for finite values of K a preliminary analysis shows that the singular limit studied here does not occur, which raises the expectation that for $K > 0$ solutions exist within the entire range $0 \le \varepsilon \le 1$, so that *So*, $\Psi - 3\pi/2$, and μ_n attain finite limits as $\varepsilon \to 1_-$. Therefore, chances are high that the singularity characterising highly-loaded massive bearings can be regularised by scrutinising a suitably defined distinguished limit $K \to 0$ as $\epsilon \to 1_-$. However, such a local analysis as available at present is still not capable of answering the original question on the existence of solutions in the space spanned by the parameters given in Table 1. Settling this issue unambiguously is also beyond the scope of the present study, but we revert to it in Section 4.2 in view of the numerical findings.

Appendix A.4. Weak singularity at inner corner of seat

The Darcy pressure P_D canonically admits a weak logarithmic irregularity at the circle $(r, z) = (1, 1)$ where the inner surface of the seat, confining the gap, intersects with its facing side: see Fig. 1(a). As exposed subsequently, it emerges because the Neumann (insulation) boundary conditions in (16) holding at the latter is suddenly superseded by the Dirichlet-type one, given by (14), at that corner. In turn, this singularity indicates that formulating the condition of insulation in such a way is probably too basic as its regularisation, necessitated on obvious physical grounds, requires their appropriate refinement, which e.g. takes into account capillary effects. However, the singularity is sufficiently weak to be not considered in the numerical scheme, see Section 4.1.

Let $[\Phi_{r0}, \Phi_{\theta 0}, \Phi_{z0}] := [\Phi_r, \Phi_\theta, \Phi_z](1, \theta, 1)$ define the (positive) values the permeability components take on at that apex. We introduce local polar coordinates R, ϑ by setting $r - 1 = R\cos\vartheta$, $1 - z = \gamma R \sin\vartheta$ with $\gamma := \sqrt{\Gamma \Phi_{z0}/\Phi_{r0}}$ so that the domain of the sinter in the vicinity of this corner is described by $0 \le \vartheta \le \pi/2$ and Taylor expansions of $\Phi_{r,\theta,z}$ in terms of sufficiently small values of R. Then the problem (15)–(17) subject to the aforementioned Dirichlet boundary condition assumes the following form in the coupled limits

$$R \to 0\,, \quad P_D \to 0\colon \quad \frac{1}{R}\frac{\partial}{\partial R}\left(R\,\frac{\partial P_D}{\partial R}\right) + \frac{1}{R^2}\frac{\partial^2 P_D}{\partial \vartheta^2} \sim -\frac{\Phi_{\theta 0}}{\Phi_{r0}}\frac{\partial^2 P_D}{\partial \theta^2} + O(R)\,, \quad \left.\frac{\partial P_D}{\partial \vartheta}\right|_{\vartheta=0} = 0\,. \tag{A.7}$$

The least-degenerate expression for P_D is governed by the Laplacian on the left-hand side of the reduced form of (15) in (A.7). Hence, $P_D \sim \mathrm{Re}\,[(d_1 \ln\zeta + e_1)\zeta + O(z^2 \ln\zeta)] + O(R^3 \ln R) \sim R\,[(d_1 \ln R + e_1)\cos\vartheta - d_1\vartheta\sin\vartheta)] + O(R^2 \ln R)$, $\zeta := R\exp(\mathrm{i}\vartheta)$, with some real functions $d_1(\theta)$, $e_1(\theta)$ of $O(1)$. At the inner edge of the seat given by $r = 1$ or $\vartheta = \pi/2$, this yields $\partial P_D/\partial r \sim d_1 \ln s + d_1 + e_1 + O(s \ln s)$ as $s := 1 - z \to 0_+$. Finally, we confirm the above remainder terms in the form of the Landau symbols by insertion of this expansion into (17) when combined with (11) and noticing the absence of cavitation for the low pressure values in the limit

$$s \to 0_+\colon \quad P_R \sim -\pi\, d_1(\theta)\, s/(2\gamma) + \Big(H'(\theta) - K\,[d_1(\theta)(\ln s - 1/2) + e_1(\theta)]\Big)\, s^2 \Big/ \Big(2H(\theta)^3\Big) + O\Big(s^3 \ln s, s^3\Big)\,. \tag{A.8}$$

That is, d_1 and e_1 appear as coefficients of eigenfunctions in the above expansions of P_D and P_R. They have to be determined numerically as they depend on the solution of the full lubrication problem (parametrised by K).

By exploiting the divergence form of the Reynolds equation (11) and the insulation conditions (16) one readily predicts zero net mass fluxes across both ends of the bearing. Specifically, in the present configuration both contributions vanish separately due to the assumed symmetry of the bearing with respect to $z = 0$, giving

$$\int_0^{2\pi} H(\theta)^3\, \frac{\partial P_R}{\partial z}(\theta, z)\,\mathrm{d}\theta = \int_0^{2\pi} H(\theta)^3 d_1(\theta)\,\mathrm{d}\theta = 0\,, \tag{A.9}$$

but *not necessarily* by a smooth continuation of the respective Neumann condition in (16) (as proposed by [25], for instance). In other words, here these together with the global condition (A.9) express the preservation of mass of the lubricant impregnating the bearing, whereas no evidence is given for the more restrictive requirement $d_1 \equiv 0$ of a locally vanishing slope of P_R and hence vanishing mass flux at the bearing edge. That is, the occurrence of the singularity expressed by (A.8) is ruled out safely only in the degenerate case $P_C = 0$ as well as the limiting one $K = 0$, but where the corresponding one of P_D stays intact. However, since we have numerically $0 < -P_C \ll 1$ in general circumstances, we also expect that $|\partial P_R/\partial z(\theta, 1)| \ll 1$.

Appendix A.5. Does discontinuous recondensation prove unavoidable in self-lubricated journal bearings?

Guided by the local mass balance (18), we elucidated in Section 2.2 that for any constellation $0 < \varepsilon < 1$, $0 \leq K$ of the two key parameters involved downstream saturation of the lubricant *may* be accompanied by the formation of a sudden jump of S and, accordingly, the pressure gradient. Without doubt, scrutinising this intriguing phenomenon of spontaneous recondensation will contribute greatly to a deeper understanding of the mechanisms leading to cavitation in the form of partial vaporisation in general. Here its emergence is described by setting the left-hand side of the Reynolds equation (11) identically to zero, according to (13). By taking into account that $\partial P_D/\partial r > 0$ in this equation, cf. Section Appendix A.1, and that $\partial S/\partial\theta \leq 0$ at incipient vaporisation, we infer that the latter takes place in the diverging part of the gap ($\theta > \pi$) and that HS increases during cavitation of a fluid particle. Unfortunately, inspection of (11) does not allow for a conclusive statement about the position or character of recondensation, in particular, whether the occurrence of discontinuities of S and the gradient of P_R there are compelling.

However, for $K = 0$ at least, a different rationale given in form of a proof below outreaches its forerunner pursued in Section 2.2 which merely relies on the conditions (18) inasmuch it predicts the imperative (rather than just possible) occurrence of discontinuities in S. It is essentially based on the decomposition of P_R into a symmetric and an antisymmetric part with respect to their dependence on the circumferential coordinate $\theta - \pi$. We stress that consistently continuous solutions cannot be ruled out for finite values of K by the possibility of their regularising effect. On the other hand, the current numerical results give preference to inevitable discontinuities of S even for moderate values of K at recondensation. We remark that so far this is found to take place slightly upstream of $\theta = 2\pi$ throughout (see the discussion of the solutions in Section 4.2).

Altogether, the introductory question raised in the headline of this section is not answered exhaustively at present. More both analytical and numerical efforts in this direction are required. We now come to its partial affirmation by the aforementioned

Proof for $K = 0$. Assume the region of cavitation to lie symmetrically with respect to the location $\theta = \pi$ of a minimum film thickness. As the product HS depends on z only, then $S = 1$ in (18) holds at both ends of this region, indicating vaporisation and recondensation, due to the respective symmetry of $H(theta)$ (and, consequently, $S(\theta, z)$). Furthermore, let P_{Rs} denote the likewise symmetric contribution to P_R, governed accordingly by the homogeneous part of (11) subject to homogeneous boundary conditions of the type (14). These are consistent with the requirement of global conservation of mass as given by (A.9) and an analogous condition holding at the boundary of the cavitation zone inside which, due to the symmetry properties of the cavitation region, P_{Rs} is to be equated with P_C, bounding P_R and hence P_{Rs} from below. Outside of it, the governing homogeneous problem is elliptic, so it is evident that P_{Rs} exhibits no local extrema there; specifically, no maxima. We then arrive at the constraint $P_C \leq P_{Rs} \leq 0$ and, given the vanishing antisymmetric remainder contribution to P_R in the region of cavitation, the rather unrealistic limitations $P_R \equiv P_C \equiv 0$ or, in the non-trivial case $P_C < 0$ of concern, $P_C \leq P_R < -P_C$. But even for this situation the upper bound for P_{Rs} together with the above global condition of zero net mass flux across the bearing edge implies locally vanishing mass flux there or $\partial P_{Rs}/\partial z \equiv 0$ for $z = 1$ (and an analogous Neumann condition holding at the cavitation boundary). Consequently, this gives again $P_{Rs} \equiv P_C \equiv 0$. By this contradiction, symmetry and, equivalently, continuity of S at recondensation on condition that $P_C < 0$ are ruled out.

The central argument of this proof rests upon the attempt to construct a not-identically vanishing symmetric contribution P_{Rs} to P_R on the double-connected region that consists of the part of the θ, z-plane describing the unwrapped gap less the fully overlapped hole where cavitation occurs. If either ε is sufficiently small so that $P_R > P_C$ throughout or cavitation is simply neglected at all, that region is single-connected. As a consequence of the exploited extremal properties of P_{Rs}, this quantity then is identically zero. In this case the resulting antisymmetry of P_R with respect

to $\theta = \pi$ is of avail in fixing the solution in the singular limit of a very long bearing. As shown next, a more exhaustive analytical progress is possible then even if cavitation is taken into account.

Appendix A.5.1. Very long bearing: $\Gamma \ll 1$

For $\Lambda \ll 1$, we define the core region where $1 - z = O(1)$ and the z-derivatives in (11) are correspondingly weak and an edge layer characterised by $1 - z = O(\sqrt{\Lambda})$ where the full form of (11) is retained so that the solution in this region can meet the Dirichlet boundary condition for $z = 1$ in (14). The properties of the resulting solution shall not be of interest here in detail with the exception that it has to satisfy conditions of matching with its counterpart governing the core region. Here we expand $P_R \sim P_{R\infty}(\theta) + o(1)$ where the drop of any (parametric) z-dependence of $P_{R\infty}$ is argued differently depending on whether cavitation occurs or not. In the second case, $P_{R\infty}$ is easily found as an odd function with respect to $\theta = \pi$ by twice integration of (11) subject to the condition of an in θ cyclic solution, expressed through the classical Sommerfeld integrals for a fully submerged, infinitely long bearing, cf. [10]:

$$P_{R\infty}(\theta) = J_2(\pi,\theta) - H^* J_3(\pi,\theta)\,, \quad H^* := J_2(\pi,2\pi)/J_3(\pi,2\pi)\,, \quad J_i(a,b) := \int_a^b \frac{\mathrm{d}\tau}{H(\tau)^i} \quad (i = 2,3)\,. \tag{A.10}$$

Any z-dependent additive contribution to $P_{R\infty}$ arising by integration is discarded in view of its antisymmetry required by the above findings concerning a bearing of finite length, here cast into conditions of formal matching with the leading-order solution in the edge layer. The extremal values of $P_{R\infty}(\theta)$ occur where $H(\theta)$ takes on the value H^*, which depends on ε.

When cavitation shall be accommodated, z-independence of $P_{R\infty}$ is due to the JFO condition taking on the forms (18). Specifically, inception of cavitation at some position $\theta = \theta_c > \pi$ demands $P_{R\infty}(\theta_c) = P_C$ and simultaneously $P'_{R\infty}(\theta_c) = 0$. This gives $HS \equiv H^* = H(\theta_c)$ during cavitation further downstream, ending at $\theta = \theta_r < \pi$, say. Hence, integrating (11) once recovers the JFO condition for (discontinuous) recondensation in (18) in the form $P'_{R\infty}(\theta_r) = 1/H(\theta_r)^2 - H(\theta_c)/H(\theta_r)^3$. Therefore, a further condition needed to determine both θ_c and θ_r in dependence of ε and P_C must again be found by leading-order matching the pressure distributions in the core and the edge region. Regarding the latter, inspection of (11) for $K = 0$ subject to the boundary condition for $z = 1$ in (14) and (A.9) shows that the integral of P_R from $\theta = 0$ to $\theta = 2\pi$ vanishes. By matching, this also holds for the core region, and the remaining condition is given by averaging $P_{R\infty}$ accordingly. Instead with (A.10), here one is finally concerned with

$$P_{R\infty}(\theta_r) = 0\,, \quad \int_{\theta_r}^{\theta_c} P_{R\infty}(\tau)\,\mathrm{d}\tau + P_C(\pi + \theta_r - \theta_c) = 0 \quad \text{as} \quad P_{R\infty}(\theta) = J_2(\theta_c,\theta) - H(\theta_c)\,J_3(\theta_c,\theta)\,, \tag{A.11}$$

to be solved for θ_c and θ_r. We expect $\pi < \theta_c < 2\pi$ and, by allowing recondensation to occur in the converging as well as in the diverging part of the gap, $0 \le \theta_r < \pi$ or $-\pi < \theta_r < 0$. Problem (A.11) might also be of interest in the study of marginal cavitation, by variation of ε.

Appendix A.5.2. Very short bearing: $\Gamma \gg 1$

The lubricant flow is less prone to cavitation if the bearing is relatively short. To put this in more precise terms, in the limit $\Gamma \to \infty$ inspection of (11) and (15) subject to (16) and (17) suggests a decrease of the pressure described by the expansion $P_D \sim \Gamma^{-1} P_0(\theta,\bar{r},z) + O(\Gamma^{-2})$ where $\bar{r} := (r-1)\sqrt{\Gamma} = O(1)$. Herein the θ-dependence of S and the function P_0 are only parametric as the lubrication problem reduces to

$$\Phi_r(1,\theta,z)\,\partial^2 P_0/\partial\bar{r}^2 + \partial\left[\Phi_z(1,\theta,z)\,\partial P_0/\partial z\right]/\partial z = 0\,, \tag{A.12}$$

subject to the periodicity and boundary conditions

$$\left.\begin{aligned} [P_0,\,\partial P_0/\partial\theta]_{\theta=0} = [P_0,\,\partial P_0/\partial\theta]_{\theta=2\pi}\,, \quad \partial P_0/\partial z\big|_{z=0} = P_0\big|_{z=1} = P_0\big|_{\bar{r}=\infty} = 0\,, \\ \left[H(\theta)^3\,\frac{\partial^2(SP_0)}{\partial z^2} - \frac{\partial(HS)}{\partial\theta} + K\Phi_r(1,\theta,z)\,\frac{\partial P_0}{\partial\bar{r}}\right]_{\bar{r}=1} = 0\,, \end{aligned}\right\} \tag{A.13}$$

the last representing the correspondingly truncated form of (11), and constraints as given by (12) or (13). The analysis of the problem given by (A.12), A.13) has not been accomplished in full detail yet, but its route is outlined as follows.

Apart from the possible z-dependence of Φ_z, (A.12) represents Laplace's equation. Therefore,its solution in terms of a Fourier series with respect to θ predicts exponential decay of P_0 when $\bar{r}$ is large, so that P_S is correspondingly small in the main part of the seat where $r-1=O(1)$ as the thickness ration Λ is kept fixed. Accordingly, matching of exponentially small terms then gives a reduced form of (15) subject to the Neumann boundary conditions in (16). We are thus confronted with a singular perturbation problem, which is regularised in case of a relatively slender seat where specifically $\Lambda = O(1/\sqrt{\Gamma})$. Then the conditions of insulation to be satisfied for a finite value of $\bar{r}$ supersede the boundary condition at infinity in (A.13).

The flow described by (A.12), (A.13) is cavitation-free if $0 < -P_C \ll 1/\Gamma$ (as $S \equiv 1$). Hence, a careful examination of this problem in another distinguished limit, namely $P_C = O(1/\Gamma)$, will shed light on the question addressed above whether discontinuous recondensation occurs even for finite values of K. This task is much easier to accomplish than solving the full lubrication problem, even though still numerically to a major extent. Efforts in this direction are currently under way. The solutions then exhibit regions of marginally cavitated flow if the value of K is below a critical threshold. Hence, their systematic investigation is essentially attended by the variation of K, besides that of ε.

Appendix A.6. Degenerate case of highly permeable seat: $K \gg 1$

A decoupling of the Reynolds from the Darcy problem (both problems then to be solved consecutively) accompanies the regular limit processes governed by $K \to 0$ as well as by $K \to \infty$. In contrast to the former discussed already extensively, however, in the latter the Darcy problem is solved first, as inferred from the predominance of the source term, proportional to K, and the (for $S \equiv 1$ inhomogeneous) Couette term in the Reynolds equation (11) over its left-hand side. More precisely, we end up with the expansion $[P_D, P_R] \sim [P_\infty(r,\theta,z), P_\infty(1,\theta,z)]/K + O(1/K^2)$ for large values of K, where the accordingly reduced form of (11) provides an inhomogeneous type of Neumann boundary conditions complementing those of the form given in (16) for the leading-order problem governing P_∞. In the so predicted flattening of the pressure variation the occurrence of (marginal) cavitation is conveniently described in terms of a distinguished limit, namely, by varying the coupling parameter KP_C, to be considered as a quantity of $O(1)$. Still the problem remains an involved nonlinear one as we allow S in the aforementioned Couette term entering the boundary condition to take on values smaller than 1 and thus being part of the solution by (13). The solution for P_∞ is unique apart from a constant determined by the ambient pressure as $P_\infty(r,\theta,1) = 0$. Finally, due to the pressure drop at a rate of $1/K$ and the then predominant Couette contribution to the gap flow the bearing looses its load carrying capability, whereas the friction factor remains finite as Petroff's law is again valid, see (20), (21) and cf. (A.3), for

$$K \gg 1: \quad So \sim So_\infty(\Gamma,\Lambda,KP_C,\varepsilon)/K + O(1/K^2)\,, \quad \mu_n \sim 3\pi/So_\infty + O(1/K)\,. \tag{A.14}$$

The specific form of the function So_∞ is determined by the parametric dependences of P_∞. Relations (A.14) demonstrate the usefulness of tackling the case $K \gg 1$ by perturbation methods.

The analysis of degenerate cases where the problems for the separate flow regions decouple is completed by mentioning the assumption of a rather thin but at same time highly permeable seat, found to be described formally by another distinguished limit process, different from that considered in Section Appendix A.5.2: let $\hat{K} := K\Lambda = O(1)$ when we have $\Lambda \ll 1$. We furthermore assume weak variations of the permeability components across the thickness of the seat in terms of their Maclaurin expansions with respect to r. In a specific extension of the analysis just outlined, we here cater to not only retaining the Couette term but also the left-hand side of (11) in its leading-order approximation. Considering this last-degenerate limit, we find the lubrication pressure P_R as represented by $\hat{P}_0(\theta,z) + o(1)$. By the first of the conditions (17), the Darcy problem then suggests a regular expansion of the form $P_D \sim \hat{P}_0(\theta,z) + \Lambda^2\hat{P}_2(\hat{r},\theta,z) + O(\Lambda^3)$ with $\hat{r} := (r-1)/\Lambda$ and the coefficient functions $\hat{P}_0$, $\hat{P}_2$ satisfying the second-order approximation of (15) reading $\Phi_r(1,\theta,z)\,\partial_{\hat{r}\hat{r}}\hat{P}_2 = \hat{D}(\theta,z) := -\partial_\theta[\Phi_\theta(1,\theta,z)\partial_\theta\hat{P}_0] + \partial_z[\Phi_z(1,\theta,z)\partial_z\hat{P}_0]$ of (15). Integration with respect to $\hat{r}$ by considering the conditions (16) of insulation yields $\Phi_r(1,\theta,z)\,\partial_{\hat{r}}\hat{P}_2 = (\hat{r}-1)\hat{D}$. Now the above distinguished limit is suggested by inserting the second of the conditions (17) into (11) as the lubrication problem is finally cast into the following modification of the Reynolds problem:

$$\frac{\partial}{\partial\theta}\left[C_\theta(\theta,z)\,\frac{\partial\hat{P}_0}{\partial\theta}\right] + \Gamma\,\frac{\partial}{\partial z}\left[C_z(\theta,z)\,\frac{\partial\hat{P}_0}{\partial z}\right] = \frac{\partial(HS)}{\partial\theta}\,, \quad C_{\theta,z} := H(\theta)^3 + \hat{K}\Phi_{\theta,z}(1,\theta,z)\,, \quad \left.\frac{\partial\hat{P}_0}{\partial z}\right|_{z=0} = \hat{P}_0\Big|_{z=1} = 0\,, \tag{A.15}$$

with $\hat{P}_0$ also subject to conditions of the type (13). Apart from $\hat{K}$, here the control parameters are Γ, ε, and KP_C, advantageously considered as an $O(1)$-quantity. Then the problem posed by (A.15) may again serve as the outset for

studying marginal cavitation in a systematic manner. For isotropic and homogeneous permeability this problem was already considered in [37, 38] under the neglect of cavitation ($S \equiv 1$); in the latter study analytical progress possible in the case of an infinitely long bearing and initiating an approximative solution in that of a three-dimensional one was achieved. Hence, the need for intensified effort in studying (A.15) is apparent: condensing the Reynolds and the Darcy problem into a single equation with essentially only two parameters governing the system behaviour involved ($\hat{K}$and ε) is attractive. At first, it is interesting to see that the lubrication pressure and, consequently, the load bearing capacity, i.e. *So*, remain finite when the seat becomes accordingly thin, in definite contrast to the prediction (A.14), which holds for (moderately) thick seats. It is remarked that the case $K \gg 1$ addressed above and that of a rather impermeable seat are formally included by this analysis when $\hat{K} \gg 1$ and $0 \geq \hat{K} \ll 1$, respectively. Therefore, the idea of studying (A.15) thoroughly definitely proves instructive from a more general viewpoint. Specifically, this includes answering the intriguing question whether solutions exists even in the limit $\varepsilon \to 1_-$.

For the implications and a discussion of specific results referring to the here addressed special cases we also refer to the numerical study [2].

Appendix B. On the failure of an iterative scheme based on Gümbel-type boundary conditions

In a first manifest attempt to solve the lubrication problem for an incompressible liquid phase, the cavitation boundary is coped with iteratively in the spirit of the basic Gümbel boundary conditions. It is instructive to focus on the inherent failure of such a procedure.

Here pointed out without the inclusion of the Darcy problem for the sake of clarity, this approach suggests the following steps: as a start, one solves the Reynolds problem by disregarding (12) and (18) and then, in the so found regions where $P_R > P_C$ and $P_R \leq P_C$, equates S with 1 and P_R with P_C, respectively. Subsequently, the (downstream) portion describing recondensation of the closed boundary confining this region is updated by solving (11) under the neglect of its left-hand side. This is followed by the consecutive step, where the Reynolds problem is solved again but by prescribing $P_R = P_C$ at that updated downstream confinement; the iteration in terms of repetitive steps becomes obvious at this point. However, convergence is doomed to fail for mainly two reasons: at first, (12) and (18) impose a weak ellipticity on the advection problem governing S in the cavitation region that cannot be accounted for by solving the associated first-order degenerate form of (11) by downstream (or upstream) integration. Secondly, and even more severe, the solution of an elliptic problem on a double-connected domain is intrinsically tied in with a singularity emerging in the extension of that region to a single-connected one. However, this cannot be coped with by the numerical solution of the Reynolds problem based upon the above iterative scheme.

Let us underpin the last finding by considering the following standard Dirichlet problem in the Euclidian plane expressed in polar coordinates r, θ rather than giving a strict mathematical proof (employing Green's function) for a function $\chi(r,\theta)$ having periodicity 2π in θ,

$$\left.\begin{aligned} 0<\rho<r<1\colon\quad & \Delta\chi \equiv r^{-1}\,\partial(r\,\partial\chi/\partial r)/\partial r + r^{-2}\,\partial^2\chi/\partial\theta^2 = 0\,, \\ r=[1,\rho]\colon\quad & \chi = [A_0,a_0] + \sum\nolimits_{i=1}^{\infty} r^n\Big\{[A_n,a_n]\cos(n\theta) + [B_n,b_n]\sin(n\theta)\Big\}\,. \end{aligned}\right\} \tag{B.1}$$

Here the coefficients A_i, a_i ($i = 0, 1, ...$) and B_i, b_i ($i = 1, 2, ...$), are assumed to be known. Then the unique solution of (B.1) is given by

$$\chi = A_0 + (a_0 - A_0)\frac{\ln r}{\ln\rho} + \sum_{n=1}^{\infty}\frac{\alpha_n\cos(n\theta)+\beta_n\sin(n\theta)}{\rho^{-n}-\rho^n}\,,\quad [\alpha_n,\beta_n] := \left\{\left(\frac{r}{\rho}\right)^n - \left(\frac{\rho}{r}\right)^n\right\}[A_n,B_n] - (r^n - r^{-n})[a_n,b_n]\,. \tag{B.2}$$

In the view of the lubrication problem considered here, the inner and outer boundaries $r = \rho$ and $r = 1$ of the annulus $0 \leq \rho < r \leq 1$ model the facing of the bearing and the cavitation interface. The corresponding boundary conditions in (B.1) and the solution in (B.2) are expressed in terms of their Fourier representations and the resultant multi-pole expansion (according to a Laurent series) around the origin $r = 0$, respectively. This solution then captures the aforementioned difficulty as by revealing the presence of an essential singularity in the origin. In potential theory, the coefficients of the logarithmic contribution and the term $1/r$ in (B.2) are interpreted as the integral flux $2\pi r\partial\chi/\partial r$ and the strength of the dipole resulting from Green's function. It is evident that analogous statements can be made for Neumann, Rubin, or accordingly mixed boundary conditions.

References

[1] Kumar V. Porous metal bearings — a critical review. Wear, 1980; 63(2):271–287.
[2] Balasoiu AM, Braun MJ, Moldovan SI. A parametric study of a porous self-circulating hydrodynamic bearing. Tribology International, 2013; 61:176-193.
[3] Morgan VT, Cameron A. Mechanics of lubrication in porous metal bearings. Proc. Conference on Lubrication and Wear, 1957; 151–157.
[4] Neumann SP. Theoretical derivation of Darcy's law. Acta Mechanica, 1977; 25(3/4):153–170.
[5] Larson RG. Derivation of generalized Darcy equation for creeping flow in porous media. Industrial & Engineering Chemical Fundamentals, 1981; 20(2):132–137.
[6] Whitaker S. Flow in porous media I: a theoretical derivation of Darcy's law. Transport in Porous Media, 1986; 1(1):3–25.
[7] Kozeny J. Über kapillare Leitung des Wassers im Boden. Sitzungsbericht der Akademie der Wissenschaften, Wien, 1927; 136(2a):271–306 (in German).
[8] Scheidegger A. The physics of flow through porous media. University of Toronto Press, 1974.
[9] Brinkman HC. A calculation of the viscous force exerted by a flowing fluid on a dense swarm of particles. Applied Scientific Research, 1949; 1A(1): 27–34.
[10] Cameron A., Mc Ettles CM. Basic Lubrication Theory. Ellis Horwwood series in engineering science, West Sussex, 3rd revised ed., 1981.
[11] Taylor GI. Cavitation of viscous fluid in narrow passages. Journal of Fluid Mechanics, 1963; 16(4):595–619.
[12] Dowson D, Taylor CM. Cavitation in bearings. Annual Review of Fluid Mechanics, 1979; 11:35–66.
[13] Swift HW. The stability of lubricating films in journal bearings. Proc. Institution of Civil Engineers (London), Minutes of the Proceedings, Part 1, 1932; 233(1932):267–288.
[14] Stieber W. Das Schwimmlager: Hydrodynamische Theorie des Gleitlagers. V.D.I. Verlag GMBH, Berlin, 1933 (in German).
[15] Floberg L. On Hydrodynamic Lubrication with Special Reference to Sub-cavity Pressures and Number of Streamers in Cavitation Regions. Acta Polytechnica Scandinavica, Mechanical Engineering Series, vol. 19, The Royal Swedish Academy of Engineering Sciences, Stockholm, 1965.
[16] Braun MJ, Hendricks RC. An experimental investigation of the vaporous/gaseous cavity characteristics of an eccentric journal bearing. ASLE Transactions, 1982; 27(1):1–14.
[17] Braun MJ. Cavitation formation and modelling for fluid film bearings: a review. Proc. Institution of Mechanical Engineers, Part J: Journal of Engineering Tribology, 2010; 224(9):839–863.
[18] Floberg L. Sub-cavity Pressures and Number of Oil Streamers in Cavitation Regions with Special Reference to the Infinite Journal Bearing. Acta Polytechnica Scandinavica, Mechanical Engineering Series, vol. 37, The Royal Swedish Academy of Engineering Sciences, Stockholm, 1968.
[19] Cuvelier C. A free boundary value problem in hydrodynamic lubrication including surface tension. Lecture Notes in Physics (Proc. Sixth Int'l Conference on Numerical Methods in Fluid Dynamics), 1979; 90:143–148.
[20] Savage MD. Cavitation in lubrication. Part 1. On boundary conditions and cavity–fluid interfaces. Journal of Fluid Mechanics, 1977; 80(4):743–755.
[21] Savage MD. Cavitation in lubrication. Part 2. Analysis of wavy interfaces. Journal of Fluid Mechanics, 1977; 80(4):757–767.
[22] Elrod HG. A cavitation algorithm. Journal of Lubrication Technology (Trans. ASME), 1981; 103:350–354.
[23] Doerr N, Gebeshuber IC, Holzer D, Wanzenböck HD, Ecker A, Pauschitz A, Franek F. Evaluation of ionic liquids as lubricants. Journal of Microengineering and Nanoelectronics (JMN), 2010; 1(1):29–34.
[24] Elrod HG, Adams ML. A computer program for cavitation and starvation problems. Proc. 1st Leeds-Lyon Symposium on Tribology, Leeds University, England, 1974; 37–41.
[25] Meurisse MH, Giudicelli B. A 3D conservative model for self-lubricated porous journal bearings in hydrodynamic steady state. Journal of Tribology (Trans. ASME), 1999; 121(3):529–537.
[26] Neacşu IA, Scheichl B, Kluwick A. Nonlinear effects due to cavitation in self-lubricated bearings. Proc. Applied Mathematics and Mechanics (PAMM), 2011; 11(1): 581–582.
[27] Vázquez C. Existence and uniqueness of solution for a lubrication problem with cavitation in a journal bearing with axial supply. Advances in Mathematical Sciences and Applications, 1994; 4(2):313–331.
[28] Bayada G, Chambat M, Vázquez C. Characteristics method for the formulation and computation of a free boundary cavitation problem. Journal of Computational and Applied Mathematics, 1998; 98(2):191–212.
[29] Bayada G, Martin S, Vázquez C. Two-scale homogenization of a hydrodynamic Elrod–Adams model. Asymptotic Analysis, 2005; 44(1/2): 75–110.
[30] Bayada G., Chambat M. On Interface Conditions for a Thin Film Flow Past a Porous Medium. SIAM Journal on Mathematical Analysis, 1995; 26(5):1113–1129.
[31] Boukrouche M, Bayada G. Mathematical model, existence and uniqueness of cavitation problems in porous journal bearing. Nonlinear Analysis: Theory, Methods & Applications, 1993; 20(8):895–920.
[32] Sahlin F, Almqvist A, Larsson R, Glavatskih S. A cavitation algorithm for arbitrary lubricant compressibility. Tribology International, 2007; 40(8):1294–1300.
[33] Dowson D, Higginson, GR. Elasto-hydrodynamic lubrication. Pergamon Press, Oxford, 1966.
[34] Brewe, DE. Theoretical Modeling of the Vapor Cavitation in Dynamically Loaded Journal Bearings. Journal of Tribology (Trans. ASME), 1986; 108(4):628–638.
[35] Mistry K, Biswas S, Athre K. Study of thermal profile and cavitation in a circular journal bearing. Wear, 1992; 159(1):79–87.
[36] Shigley JE, Mischke CR. Mechanical Engineering Design. McGraw–Hill, New York, 1989.
[37] Kumar A. Conical whirl instability of turbulent flow hybrid porous journal bearings. Tribology International, 1998; 31(2):235–243.
[38] D'Agostino V, Senatore A. Analytical solution for two-dimensional Reynolds equation for porous journal bearings. Industrial Lubrication and Tribology, 2006; 58(2):110–117.